Reply to Report #1

We would like to thank the reviewer for her or his time and the beneficial comments, which will help to improve the manuscript. Please find the replies to the referee comments below. The page and line numbers given by the referee relate to the manuscript in discussion, the numbers in our reply to the revised manuscript.

Referee comments are highlighted in **bold**, *changes* in the manuscript in *italic*.

The authors have completed a thorough revision, though I do have some remaining suggestions after consideration of which I think the manuscript will be ready for publication.

(1) I am pleased to see the inclusion of a new literature review on CRF in section 3.1. Though nitpicking, the authors may consider working in the perspective of Allen et al. 2003 and references therein into this section too, which is relevant framing for their overall discussion, in particular for the interpretation of LW CRF described in that section and page 7 (L17-19).

We totally agree with reviewer, but we were hesitant to include it, due to the different perspective (TOA and subsampling approach), which in fact represents a third methodology. However, it supports the longwave CRF discussion and we added now a paragraph in section 3.1:

"Similar issues with the cloud-free reference net irradiances are reported from satellite-based approaches (Allan and Ringer, 2003), where a subsampling of cloud-free regions is used for the estimate of CRF similar to the climatological approach. The satellite-observed cloud-free conditions are in general more stable and drier compared to the cloudy regimes assumed to be cloud-free, which affects the obtained longwave CRF values and results in inconsistencies when compared to climate model longwave CRF estimates (Allan and Ringer, 2003), where the cloud-free irradiances are calculated by neglecting clouds in the radiation scheme."

(2) I still have philosophical differences with the authors that prevent me from seeing how this study is a "reassessment" of a fundamental concept. The authors are correct that there are a variety of methods in use and that these methods are not necessarily comparable, but this is the nature of CRF, which is a hypothetical quantity. Here, the authors devote attention to a more sophisticated treatment of the albedo and I think reached some interesting conclusions. If they insist that this is a reassessment then I suppose I can live with it as it is largely stylistic point.

The reviewer is right, the concept of CRF using cloud-free fluxes is established, already by its definition. Indeed, we wanted to point out that a more "sophisticated treatment of the albedo" is recommended, as we try to show in the sections 4 & 6 by quantifying the potential impact, which suggests that a reassessment of the shortwave CRF (not the concept itself) is necessary (regarding the hypothesis in Fig. 6 and the related differences in Fig. 5). We had therefore removed the "the common concept to derive the" out of the title to bring the focus on the implementation. Also with respect to CRF in climate models and the estimate of cloud radiative feedbacks in the Arctic by partly simple albedo parameterizations e.g. in CMIP5 models; we would appreciate it if we could make this "largely stylistic point", also to draw the attention of the modeling community to this topic.

(3) In their response to my previous comments, the authors provide a sensitivity study to show the errors in CRF based on the height of the instruments. However, in the main text, there continues to be some handwaving on the treatment of the data collected at altitude, especially the LW. If the authors will not implement atmospheric corrections, I suggest that this analysis be included as supplementary material and referenced in the appropriate section.

In order to explicitly demonstrate the effect of the flight altitude, we have compiled a supplement *"Impact of flight altitude on the surface radiative energy budget and cloud radiative forcing derived from low-level flights during the ACLOUD campaign".*

Regarding an atmospheric correction:

In our point of view, an atmospheric correction is not essential for the main conclusions of the study. The analysis in the supplement clearly shows: it is reasonable to know that there is a slight bias, which was estimated in the manuscript in a quite conservative way (±5 Wm-2); but the relative contribution to the total uncertainty caused by this issue is negligible compared to other potential sources of uncertainty in the derivation of CRF. But we follow the remark of the reviewer regarding the supplement, it is an important issue of this measurement approach.

We restated the whole paragraph (now in section 5.3) and refer to the supplement:

"A special aspect of this dataset concerns the measurement strategy itself, whereby the irradiances are observed in the aircraft flight altitude (during low-level sections in average 80 m) and in various atmospheric thermodynamic profiles. Radiative transfer simulations of all available profiles during the campaign indicate that the derived total CRF in flight altitude may have an offset less than ±2 Wm-2 compared to surface-related/surface-based observation, depending on the prevailing thermodynamic profiles. Details are given in the supplement provided to this study."

(4) In the revision the authors argue that this is a study on SW processes. This is clearly stated now in the title and abstract where the focus is entirely on the SW and the LW is absent. However, within the text there is still consideration of the LW, which becomes important only at the end where the authors argue that their treatment of the SW causes the net CRF to go from strongly positive (LW dominant) to "near neutral" (perhaps "weakly positive" would be better). This is an important statement in the manuscript and it does not appear in the abstract, but is an interesting result that gives motivation to present LW calculations. I suggest including this finding in the abstract and perhaps working the concept of the balance of warming and cooling processes as a hypothesis in the introduction that warrants testing the sensitivity of SW CRF methods on net CRF results. This would set up the scope nicely for the reader.

The reviewer is right, we should have included this motivating aspect of total CRF. We added in the abstract:
"As a result, the observed total (shortwave plus longwave) CRF shifted from a clear warming effect to an almost neutral one."

An in the last paragraph of the introduction:

"This allows us, in combination with the derived longwave CRF, to analyze the general concept of a warming or cooling effect of clouds on the sea ice during the campaign and illustrate the impact of the surface albedo-cloud interaction for the total balancing effect of clouds in the springtime MIZ (section 6)."

(5) P21L19-20: Is this so? Nominally, if the boundary-layer lapse rate and surface temperature response under clearing skies is accounted for in the clear-sky term, the value of the clear-sky term should become more positive. Given that your LWD is measured at altitude, it is a bit difficult to say how things would change if the response were included.

If a cloud layer dissipates, the strongest contribution of upward emission (in a cloudy atmosphere the cloud top cooling) will be displaced to the surface, which will consequently cool. The surface will respond quicker to the new environment compared to the atmosphere, and thus, the upward irradiance (surface temperature) will quickly/strongly decrease, while the atmosphere under the assumption of any external forcing (strong large scale subsidence, advection of new air masses) will only slightly change. In case of large-scale subsidence the inversion will strengthen, and thus, the atmosphere will become warmer which will increase the downward irradiance. Thus, the net longwave irradiance will be less negative (less outgoing) in the real cloud-free atmosphere due to a colder (significantly less emitting) surface and an unchanged or slightly warmer atmosphere (same, slightly more emitting). More critical is the aspect of an in general drier cloud-free atmosphere, which can cause a compensating effect on downward irradiance (less emitting atmosphere).

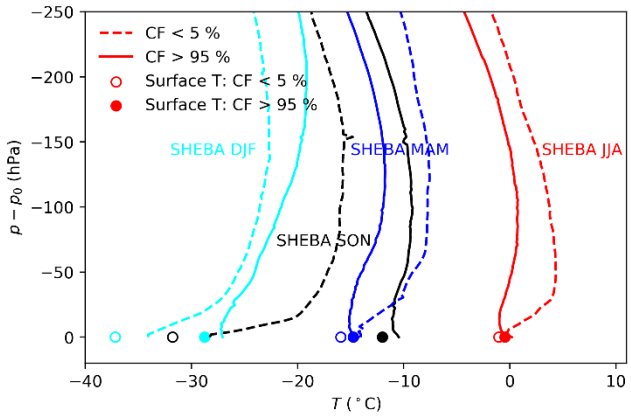

Figure 1 SHEBA seasonally averaged radiosoundings separated by cloud fraction (CF) in observations during cloudy (CF > 95 %, solid) and cloud-free (CF <5%, dashed) conditions and seasons; winter (light blue), spring (blue), summer (red) and autumn (black). Average surface temperatures during the soundings for cloud-free (open) and cloudy (filled) conditions are shown in scattered circles.

In order to underline this statement we analyzed SHEBA atmospheric soundings:

https://data.eol.ucar.edu/dataset/13.818

In Fig. 1 the seasonally averaged soundings are separated by cloudy (cloud fraction > 95 %) and cloud-free (cloud fraction < 5 %) conditions and are shown together with the temporal collocated observed averaged surface temperatures. Cloud fraction and surface temperature are obtained from:

https://data.eol.ucar.edu/dataset/13.114

Soundings without valid surface pressure have been neglected. For the average profile the net, downward and upward irradiances in assumed cloud-free conditions are simulated. The results are shown in Tab. 1.

The difference between the irradiances for cloudy profiles simulated as cloud-free and the ones for the real cloud-free atmosphere represents the average bias between the climatological and instantaneous radiative transfer based approach. In Tab. 1 the cloud-free net irradiances in the cloudy atmosphere from autumn, spring and winter are more negative (outgoing). This is likely caused by the less stable atmosphere and relatively warmer surface temperatures. Thus, the longwave CRF by the instantaneous radiative transfer based approach using the cloudy soundings for the longwave simulations of the cloud-free reference will be overestimated (stronger warming effect). In late spring and summer it will potentially

depend more on the prevailing conditions and the value of CRF itself and a weaker overestimate has to be expected. Please note that the SON might be influenced by bad statistics for clear conditions associated with the high cloud fraction in this season.

The flight altitude (during ACLOUD average 80 m) would have had a minor impact on the results (see Tab. 1).

Table 1 Simulated cloud-free longwave irradiances at the surface and in 80 m (flight altitude of an aircraft) in Wm-2 for the seasonally averaged SHEBA profiles shown in Fig. 1.

	DJF		MAM		JJA		SON	
Atmosphere:	Clear	**Cloudy**	Clear	**Cloudy**	Clear	**Cloudy**	Clear	**Cloudy**
F_net	-43.6	**-54.7**	-65.7	**-71.8**	-72.0	**-72.6**	-38.7	**-68.1**
F_dw	130.0	145.5	180.1	178.5	236.0	238.0	151.6	193.0
F_up	173.6	200.2	245.8	250.3	307.9	310.6	190.3	261.1
F_net (80 m)	-44.5	**-55.5**	-66.9	**-72.3**	-72.6	**-73.8**	-40.4	**-70.3**
F_dw (80 m)	132.2	145.8	181.1	177.6	237.8	236.2	156.3	192.1
F_up (80 m)	176.7	201.3	247.9	250.0	310.5	310.0	196.7	262.4

We restated:

"This is potentially due to the colder surface temperatures and frequent presence of surface-based temperature inversions in cloud-free conditions, causing a less negative longwave net irradiance compared to the cloud-free simulated cloudy atmosphere, which is in general less stable and exhibits a warmer surface temperature."
and:

"In late spring and summer, the surface temperature difference between cloud-free and cloudy state is smaller (Walsh and Chapman, 1998), and smaller differences between the CRF estimates of the two approaches should be expected. Therefore, the bias in the longwave CRF estimate between the climatological and radiative transfer based approach will be controlled by the prevailing conditions and the CRF itself."

However, we would prefer not to include this analysis in the already extensive manuscript, as it distracts from its focus (shortwave) and poses a new problem in making the paper more comprehensive. We had already stated,

*"From autumn to spring, the longwave CRF derived from the radiative transfer based approach **should** tend to produce a more positive (warming) CRF."*

to underline the hypothetical statement.

(6) I am not convinced that the brightness temperature measured by the KT15 at flight altitude is representative of a surface skin temperature without applying atmospheric and emissivity corrections, the latter being even more critical over the heterogeneous surface and the former being necessary

despite the narrow-band (though I know of know proven methods). I suggest at minimum drawing more attention to this assumption in the text: While the Hori article does show nadir emissivity near unity at the center of the instrument band, the range is more like ~0.96-0.995 across even the sensitivity of this narrow-band instrument and even this assumes a consistent surface type.

An important aspect concerning our study is that this emissivity assumption for the surface temperature estimate using the KT19 has almost no effect on the results presented in this study. Only for the lowest ~80m of the atmosphere the temperature is linearly interpolated between the surface brightness temperature and air temperature observed in ~80 m. The downward irradiance in ~80 m, will not be influenced by a potential biased surface temperature below that altitude.

The brightness temperature information from the KT19 consists of three components:

1. Emission from the surface with the physical surface temperature and the specific surface emissivity
2. The impact of absorption and emission of the atmosphere between the aircraft and the surface
3. The contribution of downward longwave radiation reflected at the surface in this wavelength range

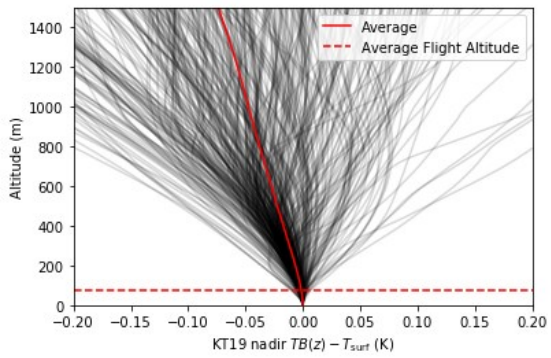

Figure 2 Simulate vertical profile of difference between nadir brightness temperature (radiance integrated from 9.6 to 11.5 µm, assuming constant spectral response of the KT19 instrument) and surface temperature (emissivity 1, only atmospheric impact) for all atmospheric profiles obtained during ACLOUD/PASCAL.

We have to point out again that our flight altitude in average was 80 m (e.g. see image in the supplement); for observations above sea ice often below that value. In Fig. 2 (this document) the atmospheric profiles obtained during ACLOUD/PASCAL which have been used for the simulations of downward irradiance are now simulated to show the vertical profile of "KT19-like" nadir brightness temperatures. A surface emissivity of 1.0 is used in order to show only the impact of atmospheric absorption between the surface and the aircraft (component 2). The small values indicate that an atmospheric correction for the absorption term between aircraft and surface is not necessary (can be neglected) in this wavelength range and the low flight altitudes. By neglecting this component, we obtain a simple formulation for the KT19 brightness temperature T_B consisting of the two remaining terms:

$$\sigma T_B^4 = \epsilon_s \sigma T_s^4 + (1 - \epsilon_s)\sigma T_{atm}^4.$$

We assume in the following a surface emissivity ϵ_s of 0.99 like in the study from Haggerty et al. (2003).

Haggerty, J. A., J. A. Maslanik, and J. A. Curry, Heterogeneity of sea ice surface temperature at SHEBA from aircraft measurements, J. Geophys. Res., 108(C10), 8052, doi:10.1029/2000JC000560, 2003.

We solve for the surface temperature T_s:

$$T_s = \sqrt[4]{\frac{T_B^4 - (1-\epsilon_s)T_{atm}^4}{\epsilon_s}}.$$

The brightness temperature of the atmosphere T_{atm} depends on the atmospheric profile, the conditions (cloudy or cloud-free) and in case of clouds on the cloud base height and optical thickness. Applying and continuous atmospheric correction would be a challenge itself.

To solve this issue appropriately to the circumstances, we have simulated in Fig. 3 all the profiles with the surface emissivity of 0.99 for cloud-free conditions (Fig. 3a) and cloudy conditions (LWP of 50 gm-2 between 200 and 400 m) (Fig. 3b).

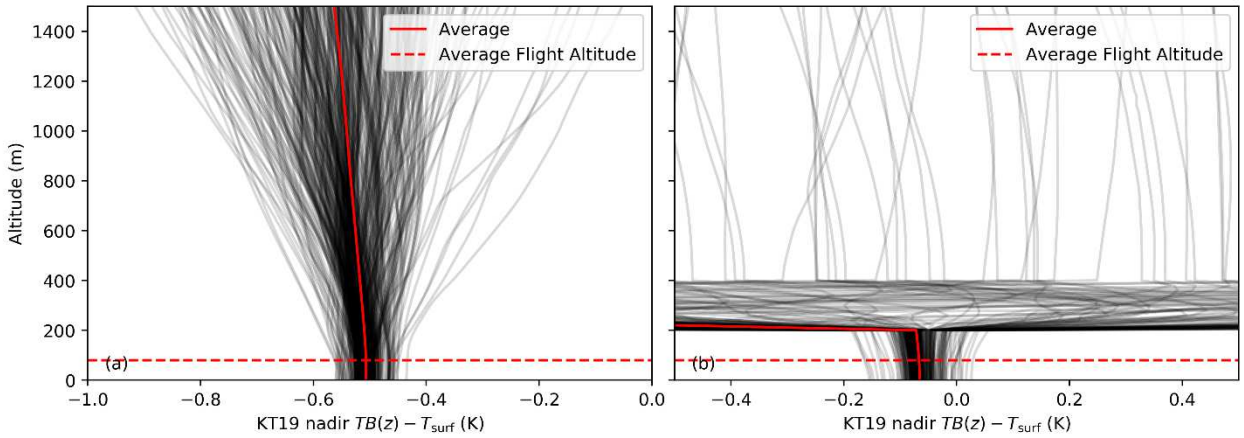

Figure 3 Same as Fig. 2, however, a surface emissivity of 0.99 was assumed. (a) Cloud-free simulated. (b) Cloudy simulated with a cloud between 200 and 400 m (LWP of 50 gm-2).

For clear-sky conditions a relatively constant averaged bias of approximately 0.5 K is indicated. Thus, in cloud-free conditions the surface physical temperature is in average 0.5 K warmer than the brightness temperature by the KT19. The majority of the flights have been conducted in cloudy conditions where a weak bias in average below 0.1 K is indicated (Fig. 3b). The impact of flight altitude can be neglected.

We restated in section 3.2:

"The temperature profile below the lowest flight altitude was linearly interpolated to the surface *brightness* temperature observed by the KT19. *For cloudy conditions radiative transfer simulations (assuming a surface emissivity of 0.99, Hori et al., 2006) of the observed atmospheric profiles indicate that neglecting an atmospheric correction for cloudy conditions is justified and the brightness temperature of the KT19 can be related to the surface temperature causing uncertainties below ±0.2 K. During cloud-free conditions a correction of 0.5 K have been added to the brightness temperature (average value obtained from radiative transfer simulations) to compensate for atmospheric and surface emissivity effects. The impact of flight altitude (average 80 m) can be neglected and potential surface temperature uncertainties hardly affect the downward irradiance simulated in flight altitude."*

(7) P5L26: "location and time" instead of "location"; P21L7: "enables" to "enables us to"

Corrected.

Additional changes:

- We included the citation of the now published dataset with the retrieved quantities of LWP equivalent, CRF and cloud-free albedo required to reproduce the results of this study (in "Data availability") (https://doi.org/10.1594/PANGAEA.909289).

- We updated the citation of the SHEBA data used in Fig. 6 to the more formal/general NCAR/UCAR EOL data page https://data.eol.ucar.edu/dataset/13.818 , not the “acknowledgement way” as described on https://atmos.uw.edu/~roode/SHEBA.html

Reply to Report #2

We would like to thank the reviewer for her or his time and the beneficial comments, which will help to improve the manuscript. Please find the replies to the referee comments below. The page and line numbers given by the referee relate to the manuscript in discussion, the numbers in our reply to the revised manuscript.

Referee comments are highlighted in **bold**, *changes* in the manuscript in *italic*.

Overall: The manuscript is significantly improved by the authors' edits and it is worth publishing. However, it still requires major revision. Although the writing is generally understandable, the entire manuscript should be reviewed and edited for grammar and clarity. Overall, the main issue with the manuscript is the organization, which makes it extremely difficult to follow. It should be possible to easily find the results of the paper and discussion of those results, which is currently very difficult since they are intermixed with introductory material and methods.

Please rewrite the statement of what this work does on page 3, lines 8-10, to be more general and relate better to what is actually done in the paper. The current lines suggest that this work specifically focusses on the two processes that change the surface albedo in cloudy conditions (1) cloud-induced weighting of the transmitted downward irradiance to smaller wavelengths and 2) a shift from direct to diffuse irradiance in cloudy conditions). However, this seems to be too specific based on the results presented. A better statement would be that this work evaluates the effects of surface albedo-cloud interactions on CRF, including the impact of areal vs local albedo and exploration of the dependence of surface albedo on cloud LWP for different surface types, and during ACLOUD; and that this work presents the effect of surface albedo-cloud interactions on CRF during ACLOUD. This statement should be parallel with what is in the abstract and conclusions.

The reviewer is right. This last paragraph of the introduction did not clarify the main aspects of this paper (and structure) and we have accordingly restructured it. Please see the track change file.

Sections 3 and 4: These sections intermix introductory material, methods, and results. To my read, Section 3.1 is introductory material, Section 3.2 is definitions, Section 3.3 is an uncertainty estimate for a particular source of error, and Section 3.4 presents an interesting result that is perhaps novel? Section 3.4.1 seems to give an overall estimation of uncertainty and it is unclear to me why it is a subsection of 3.4. Section 3.5 refers to the processes (1) and (2) above and, as such, would seem to be a main result of the paper, so why is it buried here? Why are all these subsections grouped together in one section? Section 4.1 seems to be methods again. Section 4.1.1 is entitled "Application to the observations," but various things have already been applied to various observations, so a more descriptive title is needed; perhaps "Dependence of surface albedo on cloud LWP for ACLOUD measurements." The Section 4.2 title, "Correction of CRF," is also insufficiently descriptive and should be changed.

Please put introductory material (Section 3.1) into the introduction, or its own section. Please consider having a section on methods, that groups all methods together (e.g. 2.2, 3.2, 4.1), and a section on uncertainty (which would include Sections 3.3 and 3.4.1.) The results seem to be contained in Sections 3.4, 3.5, 4.1.1 and 4.2, so these should be grouped together. Furthermore, section titles should make

clear that 3.5 represents a model study related to the two processes showing how broadband albedo changes with LWP for different surface types (related to process 2) and attenuation of incident irradiance by clouds (related to process 1), whereas 4.1.1 shows how broadband albedo changes with LWP for the ACLOUD measurements (related to process 2).

We have invested an extensive amount of time to restructure the manuscript to meet the requirements and try out various arrangements, but it was quite delicate due to the linkage between methods and results. We tried to give the section more descriptive titles.

The new structure reads:

1 Introduction
2 The concept of cloud radiative forcing (CRF)
2.1 Review of approaches to derive the CRF
2.1.1 Estimating net irradiance in cloud-free conditions
2.1.2 Handling of surface albedo
2.2 Definitions and process handling
2.2.1 Longwave CRF
2.2.2 Shortwave CRF
3 Observations and modeling
3.1 Airborne measurements and instrumentation
3.2 Radiative transfer simulations
3.3 Necessity of a local thermodynamic profile for the estimate of CRF
4 Modeling the surface albedo-cloud interaction
4.1 Impact of clouds on surface albedo
4.2 Impact on shortwave CRF
4.3 Seasonal cycle of shortwave CRF
5 Refining the derivation of shortwave CRF
5.1 Considering surface albedo heterogeneities and horizontal photon transport
5.2 Retrieval of cloud-free albedo from cloud-sky observations
5.3 Uncertainties
6 Impact of surface albedo-cloud interaction on the CRF during ACLOUD
7 Summary and conclusions
Appendix A: Transmissivity-based retrieval of LWP equivalent

We tried to follow the reviewer`s advice by putting the literature overview right after the introduction. We avoided an inclusion in the introduction due the resulting length. It was also quite important to us to show our approach in the "Definitions section" right after the literature overview.

We "dug" the modeling study on surface albedo cloud interaction out and gave it an own section to emphasize the importance for this study (**"…main result of the paper, so why is it buried here?"**) and not include it in a results section, where it might be buried again ("**The results seem to be contained in Sections 3.4, 3.5, 4.1.1 and 4.2, so these should be grouped together.**").

Regarding the "Methods" section we decided to move "Necessity of a local thermodynamic profile…" to "Radiative transfer simulations" as it fits perfectly to the already discussed handling of the temperature profiles described in this section. However we think this subsection **("Section 3.3"**) is not "**an uncertainty**

estimate for a particular source of error", moreover it represents an important aspect of this measurement approach and the studied processes in the MIZ.

Left over are 5.1, 5.2 and a section combining now all uncertainties of the presented retrievals and issues regarding this dataset (section 5.3). These three subsections were grouped into kind of a "Methods" section "Refining the derivation of CRF", although the content already "**presents an … result".**

Same issue with the section "Retrieval of cloud-free albedo from cloud-sky observations", which contains already an application to ACLOUD data for one flight.

However, putting the section "Retrieval of cloud-free albedo…" already in a "methods" section, while the reasons ("modeling the surface albedo-cloud interaction") are given later in the results section, would have been hard to motivate ("**Please consider having a section on methods, that groups all methods together (e.g. 2.2, 3.2, 4.1)**", **The results seem to be contained in Sections 3.4, 3.5, 4.1.1 and 4.2, so these should be grouped together.**).

We have really struggled with the rearrangement and hopefully achieved a clearer outline. Please see the track change file/revised manuscript.

Specific comments:
Please put a horizontal space (extra line break) between paragraphs or begin new paragraphs with an indent so the reader can tell when a paragraph ends.

Corrected.

Page 6 last line – Page 7 lines 1-2: Please delete these sentences. I do not see the point of them, as the current work would also fall into the category of being limited in comparability to previous results due to a different means of computing CRF. Furthermore, the current work relies on aircraft flights, which are not available to many of the previous studies and therefore could not be applied to them.

We agree, but on the other hand this is a pretty important aspect we want to point out in this section. We changed the paragraph to:

"The potential systematic differences in shortwave CRF estimates associated with the respective assumed surface albedo motivate to provide a quantitative measure of these differences as well as an improved solution for the albedo reference to enable a more harmonized understanding of CRF."

However, we do not understand why our results and methods are not applicable to other studies? In fact, on the contrary, our approach would even benefit from high quality ground-based remote sensing (LWP retrievals). The cloud-free albedo retrieval should be easily applicable for common long-term observations (like Intrieri et al., 2002; Shupe and Intrieri, 2004; Dong et al., 2010; Sedlar et al., 2011; Miller et al.,2015) or the current MOSAiC campaign. The parameters required for the Gardner and Sharp parameterization: broadband surface albedo, LWP, SZA are available and even the impurity content of snow could be estimated from snow samples.

If needed for inhomogeneous surface conditions, the areal averaged albedo can be obtained from helicopter measurements or kind of "line albedo" measurements (like during SHEBA, Perovich et al. (2002)) for example, and would be helpful also for coastal sites with a strong reported gradient in albedo (impact discuss in Ricchiazzi and Gautier (1998) and Kreuter et al. (2014)).

As we show now in the supplement (reply to Report #1) our airborne observations are no measurements from space and we can reasonably relate the results to the surface REB.

"…as the current work would also fall into the category of being limited in comparability to previous results..": Of course, because we present a method with which comparability based on one distinct reference value (cloud-free albedo) would be given, not influenced by the cloud properties itself or fits or extrapolation of conditions a few days/weeks ago. Without comparability; what is the use of another dataset that gives another vacuous number of 36.9 Wm-2 total CRF…

Page 7 lines 4-6: Please delete these lines or change them to "Below, we derive the … CRF. Our approach is unique in that we use a continuous … cloudy conditions." Please add to the sentence any aspect of using the areal-averaged albedo that is unique to this work. E.g, if it's true you could say, " Below, we derive the … CRF. Our approach is unique in that we use a continuous … cloudy conditions, and in that we account for horizontal photon transport through using the areal-averaged albedo to compute downward shortwave fluxes, as discussed below."

We restated this section accordingly:

"Below, we derive the radiative transfer based instantaneous CRF. Our approach is unique in that we use a continuous estimate of the cloud-free surface albedo of snow and ice obtained from observations in cloudy conditions, and in that we account for horizontal photon transport through using an areal-averaged albedo to compute the downward shortwave irradiances, as discussed below."

Pages 7-8
In these equations, the two alphas in Eqn. 7 are later replaced with two non-equal terms, which is not mathematically correct. You can avoid this and simplify by adding the subscripts "all" and "cf" to the relevant alphas in Eqn (8). With this change, Eqn (10) could then replace Eqn (9), which would no longer be needed. The text from lines 19-22 could then be moved to just before Eqn (8) to provide the necessary context, after revising it to read "The surface albedo changes for … Warren (1982). Thus, the measured surface albedo has been separated … alpha_cf."

We have rearranged the section accordingly to eliminate equation 9 (old manuscript) and shorten the section. Please see the track change version.

Page 11, line 12: reference needed after "(increasing grain size)."

We added in P. 13 L.12 (old manuscript) the citations from Warren (1982) and Gardner and Sharp (2010) and slightly changed the sentence:

"The impact of snow properties on the spectral surface albedo is characterized by the fact that with decreasing SSA (increasing effective grain size) the absorption at longer wavelengths increases (Warren, 1982; Gardner and Sharp, 2010)."

Lines 16-19: references are needed.

We added a reference:

"Two processes influencing the broadband snow albedo are related to the transition from cloud-free to cloudy atmospheric conditions. In an overcast atmosphere with clouds of sufficient optical thickness,

mainly diffuse radiation illuminates the surface as compared to cloud-free conditions, when the direct shortwave radiation dominates *(Gardner and Sharp, 2010)*."

Also, this text through page 14 line 2 seems to be an expansion of information that was given in the introduction and should therefore be moved to the introduction. Retain here only enough information needed to introduce and discuss the results (e.g. "Fig. 5 shows the effect of …").

In the introduction we introduce the general concept by explaining the two processes relevant for the main conclusion of the paper. In our point of view, such details would distract in the introduction. However, where it is absolutely necessary to understand the processes shown in Fig. 3 and 4 (new manuscript) and following conclusions in the next sub-sections, the reader would have to look up 10 pages earlier. We think it would be best to have this information where it is needed (in the following lines) and where the effects are illustratively shown (main reason for this section 4.1).

Section 4.2 seems like an important section but the results shown in Fig. 10 are not described sufficiently. The caption/text and the legend do not agree. What is "Corrected delta F?" This phrase occurs nowhere else in the paper.

We have described/discussed the features more extensively (providing more statistical background) and adjusted the inconsistent labels in Fig. 10 and avoided "corrected". We apologize for this inconsistences. Please see the track change file.

The conclusion (page 20) slowly transitions from a description of the literature, which is not always referenced (lines 12-14, line 17) to results from the current work. Is line 18-20 from the literature or current work? Please reference all statements that are already known and start a new paragraph for the findings of this work, which should begin with a sentence using language such as "we find" or "our results show" to make this clear.

We have slightly restructured the conclusion (now "Summary and conclusions") and used bullet points to separate the single topological sections. We included citations for the general motivational sentences at the beginning of each section in order to separate our work more clearly from the literature.

lines 12-14: We added:

"In the transition region between open ocean and closed sea ice (the MIZ), the thermodynamic state of the atmosphere changes on horizontal scales of a few kilometers (Lampert et al., 2012), which influences the cloud-free reference state and the resulting simulated radiative field."

line 17: *"Variability in sea ice concentration is closely linked with fluctuations in surface albedo."* We think this statement is so general and obvious that we do not see a reason for a citation.

line 18-20: We added:
"The derivation of downward shortwave irradiances under cloud-free conditions in heterogeneous surface albedo conditions requires an estimate of the effective areal average surface albedo, determining the multiple scattering on large spatial scales (e.g., Kreuter et al., 2014)."

Additional changes:

- Due to the editing for reasons of clarity there have been slight changes in the legend of Fig. 3 and 10. In Fig. 6 the icons have been enlarged.

Reassessment of shortwave surface cloud radiative forcing in the Arctic: Consideration of surface albedo – cloud interactions

Johannes Stapf[1], André Ehrlich[1], Evelyn Jäkel[1], Christof Lüpkes[2], and Manfred Wendisch[1]

[1]Leipzig Institute for Meteorology (LIM), University of Leipzig, Germany
[2]Alfred Wegener Institute, Helmholtz Centre for Polar and Marine Research, Bremerhaven, Germany

Correspondence: Johannes Stapf (johannes.stapf@uni-leipzig.de)

Abstract. The concept of cloud radiative forcing (CRF) is commonly applied to quantify the impact of clouds on the surface radiative energy budget (REB). In the Arctic, specific radiative interactions between microphysical and macrophysical properties of clouds and the surface strongly modify the warming or cooling effect of clouds, complicating the estimate of CRF obtained from observations or models. Clouds tend to increase the broadband surface albedo over snow or sea ice surfaces, compared to cloud-free conditions. However, this effect is not adequately ~~represented~~ considered in the derivation of CRF in the Arctic so far. Therefore, ~~in this study we quantify~~ we have quantified the effects caused by surface albedo-cloud interactions over highly reflective snow or sea-ice surfaces on the CRF using radiative transfer simulations and below-cloud airborne observations ~~in~~ above the heterogeneous springtime marginal sea ice zone (MIZ) during the Arctic CLoud Observations Using airborne measurements during polar Day (ACLOUD) campaign. The impact of a modified surface albedo in the presence of clouds, as compared to cloud-free conditions, and its dependence on cloud optical thickness is found to be relevant for the estimation of the shortwave CRF. A method to consider this surface albedo effect on CRF estimates by continuously retrieving the cloud-free surface albedo from observations under cloudy conditions is proposed, using an available snow and ice albedo parameterization. ~~Applying ACLOUD data it is shown~~ Using ACLOUD data reveals that the estimated average shortwave cooling ~~effect~~ by clouds almost doubles over snow and ice covered surfaces (-62 $\mathrm{W\,m^{-2}}$ instead of -32 $\mathrm{W\,m^{-2}}$), if surface albedo-cloud interactions are considered. As a result, the observed total (shortwave plus longwave) CRF shifted from a warming effect to an almost neutral one. Concerning the seasonal cycle of the surface albedo it is demonstrated that this effect enhances shortwave cooling in periods where snow dominates the surface, and potentially weakens the cooling by optical thin clouds during the summertime melting season. These findings suggest that the surface albedo-cloud interaction should be considered in global climate models and in long-term studies to obtain a realistic estimate of the shortwave CRF ~~in order~~ to quantify the role of clouds in Arctic amplification.

1 Introduction

Interdisciplinary research conducted within the last decades has led to a broader, but not yet complete understanding of the rapid and, compared to mid-latitudes, enhanced warming in the Arctic (so-called Arctic amplification) (Gillett et al., 2008; Overland et al., 2011; Serreze and Barry, 2011; Stroeve et al., 2012; Jeffries et al., 2013; Cohen et al., 2014; Wendisch et al.,

2017). Since the numerous interactions of physical processes, responsible for Arctic amplification, are intertwined and difficult to observe, climate models are needed to quantify the individual contributions of feedback processes to Arctic climate change (Screens and Simmonds, 2010; Pithan and Mauritsen, 2014). However, the model results show a large spread in representing the feedback mechanisms. One prominent example is the cloud radiative feedback, which includes the effects of an increasing cloud amount in the Arctic, balancing between the potential increase of both longwave downward radiation (positive) and cloud top reflectivity (negative). To enable reliable projections of future climate changes in the Arctic, the understanding of the individual physical processes and feedback mechanisms causing Arctic amplification is required (Pithan and Mauritsen, 2014; Goosse et al., 2018), as well as observations of how clouds influence the Arctic surface radiative energy budget (REB).

To quantify the radiative effect of clouds on the REB, the concept of cloud radiative forcing (CRF, expressed as ΔF) is defined as the difference between the net total (shortwave plus longwave) radiative energy flux densities,

$$F_{\mathrm{net}} = F^{\downarrow} - F^{\uparrow}, \tag{1}$$

also called irradiances, in all-sky ~~conditions~~ ($F_{\mathrm{net,all}}$) and cloud-free ($F_{\mathrm{net,cf}}$) conditions (Ramanathan et al., 1989):

$$\Delta F = F_{\mathrm{net,all}} - F_{\mathrm{net,cf}}. \tag{2}$$

A warming effect at the surface will be caused by clouds if the net radiative flux densities in a cloudy atmosphere are larger than in corresponding cloud-free conditions.

Long-term ground-based observations of CRF in the Arctic (Walsh and Chapman, 1998; Shupe and Intrieri, 2004; Dong et al., 2010; Miller et al., 2015) showed that in the longwave wavelength range (4 – 100 µm) clouds tend to warm the surface. The magnitude of the warming is influenced by macrophysical and microphysical cloud properties (e.g., Shupe and Intrieri, 2004) and by regional characteristics (Miller et al., 2015) and climate change (Cox et al., 2015). In the ~~solar spectral range~~ shortwave spectral range (0.2 – 4 µm), clouds rather cool, whereby the strength and timing over the year is determined, besides cloud microphysical properties, by the solar zenith angle (SZA) and the seasonal cycle of surface albedo (e.g., Intrieri et al., 2002; Dong et al., 2010; Miller et al., 2015). However, the required cloud-free reference ($F_{\mathrm{net,cf}}$) poses a serious problem to all observations in the cloudy Arctic (Shupe et al., 2011), as the unknown thermodynamic and surface albedo conditions in cloud-free environments ~~is~~ are modified by the presence of clouds itself.

Low-level clouds in the Arctic boundary layer cause elevated temperature inversions, modified thermodynamic profiles, and changed turbulent energy and momentum fluxes, as compared to a cloud-free atmosphere. In addition, the clouds modify the surface energy budget by the two competing effects of longwave warming and shortwave cooling~~, with consequences for the surface temperature and turbulent fluxes~~. This results in two typical states of thermodynamic profiles (Tjernström and Graversen, 2009) and longwave radiative irradiances (Stramler et al., 2011; Wendisch et al., 2019) observed in the Arctic winter. As demonstrated by Walsh and Chapman (1998), the surface temperature change accompanied by the transitions from cloudy to clear skies is not an instantaneous effect; it rather occurs in the range of hours to days and potentially only advanced boundary layer models might ~~be able to~~ predict the transition between the two states after a given time.

Besides temperature and humidity changes, clouds modify the illumination and reflection of the surface. For highly reflecting snow surfaces, radiative transfer simulations show that two processes are crucial: (i) A cloud-induced weighting of the

transmitted downward irradiance to smaller wavelengths, causing an increase of shortwave surface albedo, and (ii) a shift from mainly direct to rather diffuse irradiance in cloudy conditions, which decreases the shortwave albedo (Warren, 1982). Observations have shown that ~~, in general,~~ there is a tendency that the surface albedo is larger in cloudy, compared to cloud-free conditions (e.g., Grenfell and Perovich, 2008), ~~and~~ which was demonstrated for a seasonal cycle by Walsh and Chapman (1998) for highly ~~reflecting~~ reflective surface types. Radiative transfer simulations ~~open up the possibility to tackle~~ enable to evaluate in detail the processes involved in the cloud-related surface albedo changes. Both processes (i and ii), have been parameterized for snow and ice, for example by Gardner and Sharp (2010) based on simulations. However, their impact on estimates of CRF in the Arctic have not yet been ~~evaluated.For this purpose we deploy combined snow surface albedo model and atmospheric radiative transfer simulations and illustrative low-level (below cloud) airborne observations of the REB in the marginal sea ice zone (MIZ)during the Arctic CLoud Observations Using airborne measurements during polar Day (ACLOUD) campaign (Wendisch et al., 2019)~~assessed.

In this study, available approaches to derive the CRF are reviewed, focusing on processes involved in the transition between cloudy and cloud-free state (section 2). After an introduction of the airborne observations, the instrumentation and the radiative transfer simulations (section 3), ~~available approaches to derive the CRF are reviewed in section ??. Furthermore, in this section the interaction between spectral surface albedo and cloud optical thickness and its importance for~~ we combine a snow surface albedo model with an atmospheric radiative transfer model to show how the surface albedo of different snow and ice types is modified by the presence of clouds (section 4). The potential impact of this surface albedo-cloud interaction on the estimate of shortwave CRF is analyzed ~~and quantified. In section ?? a method is introduced~~ depending on the surface type and seasonality. The application of an areal-averaged surface albedo for the radiative transfer simulations of the shortwave cloud-free irradiances (section 5.1) enables us to derive the CRF in the heterogeneous albedo environment of the marginal sea ice zone (MIZ) using low-level (below cloud) airborne observations of the REB during the Arctic CLoud Observations Using airborne measurements during polar Day (ACLOUD) campaign (Wendisch et al., 2019). A method to retrieve the shortwave surface albedo in the hypothetical cloud-free atmosphere from measurements under cloudy conditions, by using ~~an available~~ the above mentioned snow and ice albedo parameterization from Gardner and Sharp (2010) and a shortwave transmissivity-based retrieval of cloud liquid water path (Appendix A) ~~. An application of this approach to ACLOUD airborne observations is presented, extending available REB and CRF datasets/observations in the Arctic including horizontal variability in the heterogeneous MIZ.~~

2 ~~Observation and modelling~~

1.1 ~~Airborne measurements~~

~~The cloudy atmospheric boundary layer in the MIZ north west of Svalbard was studied using the research aircraft Polar 5 and Polar 6 from the Alfred-Wegener Institute (AWI)during the ACLOUD campaign performed in spring between 23 May and 26 June 2017 (Wendisch et al., 2019). Part of the flights were dedicated to characterize the near-surface radiative energy budget below ABL clouds. From all flights, 16 hours of data measured below an altitude of 250 (average 80) covering a distance of 3700 km are investigated in this paper. The sea ice concentration observed along the low-level flights by instruments mounted~~

on the aircraft is displayed in Fig. 1, together with a Moderate Resolution Imaging Spectroradiometer (MODIS) satellite image showing the sea ice distribution representative for the campaign. During the ACLOUD period, the location of the MIZ, indicated by the contour lines of average sea ice fraction (I_f), was almost stationary (Knudsen et al., 2018). The sea ice was more compact (higher concentration) north of 81° N geographic latitude, and rather heterogeneous towards the west and the open ocean. The majority of flights (66 %) were over sea ice ($I_\mathrm{f} > 80$ %), leaving about 17 % over the MIZ as well as 17 % over open ocean ($I_\mathrm{f} < 15$ %). As the dataset is merged from different flights covering about six weeks of measurements, it comprises various sea ice characteristics and synoptic situations (Knudsen et al., 2018). However, the data set is still limited and should be considered as a snapshot of the late spring conditions in this region.

1.1 Instrumental payload

MODIS satellite image on 1 June 2017, representing the typical sea ice distribution during the ACLOUD campaign. All low-level flight sections during the ACLOUD campaign are indicated with the sea ice fraction derived from airborne observations. Red (80 %) and light-blue (15 %) contours indicate the campaign average sea ice fraction from daily sea ice data (Spreen et al., 2008). The comprehensive instrumentation of Polar 5 and Polar 6 during the ACLOUD campaign is described by Wendisch et al. (2019) and by Ehrlich et al. (2019b). In this paper, shortwave and longwave , upward and downward broadband irradiance have been analyzed from measurements with a frequency of 20 obtained from two sets of Pyranometer (0.2-3.6) and Pyrgeometer (4.5-42). From these irradiance data the net irradiance and surface albedo have been derived. The processing of the Pyranometer and Pyrgeometer data (Stapf et al., 2019a), which were used to derive the REB from ACLOUD observations, is detailed in Ehrlich et al. (2019b). Surface brightness temperature was obtain by a Kelvin Infrared Radiation Thermometer (KT–19) (Stapf et al., 2019a). The ice fraction I_f along the flight track was estimated from measurements of a digital camera equipped with a hemispheric lens. The geometrically calibrated images were obtained with a sampling frequency of 6 ; from the images the cosine-weighted sea ice concentration was calculated (Jäkel et al., 2019). The local atmospheric thermodynamic state, including air temperature and relative humidity, was determined by dropsondes (Ehrlich et al., 2019a) and aircraft in situ observations (Hartmann et al., 2019) during ascents and descents in the vicinity of the low-level flight sections.

1.1 Radiative transfer simulations

The radiative transfer simulations for the cloud-free conditions were performed with the libRadtran package (Emde et al., 2016) using the one-dimensional, plane-parallel discrete ordinate radiative transfer solver DISORT (Stamnes et al., 1988) and the molecular absorption parameterization from Kato et al. (1999) for the shortwave spectral range (0.28–4), and from Gasteiger et al. (2014) for the longwave wavelengths range (4–100). The aerosol particle optical thickness was neglected in the simulations, because the full column aerosol information were not available for low-level flights in cloudy conditions. Therefore, the estimated CRF needs to be considered as direct aerosol plus cloud radiative forcing.The atmospheric state, required as input for the radiative transfer simulations to derive the CRF, was based on radiosoundings performed in Ny-Ålesund (Svalbard) (Maturilli, 2017a, b) and onboard Polarstern (Schmithüsen, 2017), which were partly spatially and temporally separated from the airborne observations by several hundred kilometres and up to three hours. Hence, profiles from in situ measurements of temperature and relative

humidity on board of both aircraft and, if available, dropsonde measurements from the Polar 5 aircraft were used to replace the radiosounding layers by the local atmospheric profiles. The atmospheric levels below flight altitude were linearly interpolated to the surface temperature observed by the KT-19 assuming an emissivity of unity. The assumption of the black-body emissivity is justified by the high spectral emissivity for nadir observations in this wavelength range (Hori et al., 2006). The sub-Arctic summer profile (Anderson et al., 1986) was used to complete the profiles including gas concentrations up to 120 altitude. Daily ozone concentrations in the flight region of ACLOUD were considered and obtained from . The high vertical resolution of the in situ observations was reduced for the radiative transfer simulations to 30 below 1000 and stepwise increases to 5 at 120 altitude. The surface albedo was obtained from upward and downward looking pyranometers and a method described in section ??.Spectral surface albedo values for the sensitivity study in section ?? were simulated using the spectral Two-streAm Radiative TransfEr in Snow model (TARTES) (Libois et al., 2013). 3D radiative transfer simulations for the albedo smoothing kernels applied in section 5.1 and the appendix A were performed with the open-source Monte Carlo Atmospheric Radiative Transfer Simulator (MCARaTS)(Iwabuchi, 2006; Iwabuchi and Kobayashi, 2008). is introduced (section 5.2). This allows us, in combination with the derived longwave CRF, to analyze the general concept of a warming or cooling effect of clouds on the sea ice during the campaign and to illustrate the impact of the surface albedo-cloud interaction for the total balancing effect of clouds in the springtime MIZ (section 6).

2 Estimate The concept of surface cloud radiative forcing (CRF)

2.1 Common Review of approaches to derive the CRF

To derive the CRF from ground-based observations, simultaneous measurements of net irradiances in cloudy all-sky, i.e. cloudy ($F_{\mathrm{net,all}}$) and cloud-free ($F_{\mathrm{net,cf}}$) conditions would be needed. From a practical point of view it is impossible to simultaneously measure in cloudy and in cloud-free conditions at the same location and time. Therefore, the common approach is to measure net irradiances in cloudy conditions, and estimate the respective net irradiances in the hypothetical cloud-free atmosphere. For ground-based observations, two general approaches have been realised applied in the past to estimate the $F_{\mathrm{net,cf}}$.

2.1.1 Estimating net irradiance in cloud-free conditions

Firstly, a radiative transfer based approach transfer-based approach is used, which aims to estimate the instantaneous CRF by simply removing discarding the cloud in the simulations the cloud from the observed atmosphere, neglecting changes of the thermodynamic state over time or atmospheric properties over time and differences of the cloudy and cloud-free surface albedo (Intrieri et al., 2002; Shupe and Intrieri, 2004; Sedlar et al., 2011; Cox et al., 2015; Wang et al., 2018) and partly Miller et al. (2015) (as described by Intrieri et al. (2002); Shupe and Intrieri (2004); Sedlar et al. (2011); Cox et al. (2015); Wang et al. (2018) and partly by Miller et al. (2015) using cloud-free albedo observations)surface albedo observations. A second, more rather climatological approach (Walsh and Chapman, 1998; Dong et al., 2010; Cox et al., 2016) uses observations in cloud-free conditions to extrapolate the cloud-free state during cloudy periods. In this technique, fitting algorithms either fitting algorithms for the estimate

of cloud-free downward irradiance from Long and Ackerman (2000) and Long and Turner (2008) are applied, or ~~observed~~ the average cloud-free ~~/cloudy irradiances are averaged~~ irradiances are used to represent monthly ~~values (Walsh and Chapman, 1998) and partly Dong et al. (2010) (averaging~~ reference values as implemented by Walsh and Chapman (1998) and partly by Dong et al. (2010) wher the upward longwave irradiance ~~)~~is averaged. The cloud-free, shortwave upward irradiance can be obtained from methods described in Long (2005).~~In all these methods~~

In these approaches, the physical processes involved in the estimate of $F_{\mathrm{net,cf}}$ are represented differently, ~~resulting in~~ which leads to systematic differences in the ~~derived CRFof the individual approaches~~resulting CRF. From autumn to spring, the longwave CRF derived from the radiative ~~transfer based~~ transfer-based approach should tend to ~~produce~~ simulate a more positive (warming) longwave CRF compared to the climatological approach. This is potentially due to the ~~in general colder cloud-free surface temperatures , the~~ colder surface temperatures and frequent presence of surface-based ~~and dissipation of elevated~~ temperature inversions in cloud-free conditions~~. In~~ , causing a less negative longwave net irradiance compared to the cloud-free simulated cloudy atmosphere, which is in general less stable and exhibits a warmer surface temperature. In late spring and summer, the surface temperature difference between cloud-free and cloudy state is smaller (Walsh and Chapman, 1998), and smaller differences between the CRF estimates of the two approaches should be expected. Therefore, the ~~difference in the~~ bias in the longwave CRF estimate between the climatological and radiative ~~transfer based approach will depend on~~ transfer-based approach is controlled by the prevailing conditions ~~controlled by a neutral or potentially even cooling CRF .The~~ and the CRF itself.

Similar issues with the cloud-free reference net irradiances are reported from satellite-based approaches (Allan and Ringer, 2003), where a subsampling of cloud-free regions is used for the estimate of CRF similar to the climatological approach. The satellite-observed cloud-free conditions are in general more stable and drier compared to the cloudy regimes assumed to be cloud-free, which affects the obtained longwave CRF values and results in inconsistencies when compared to climate model longwave CRF estimates (Allan and Ringer, 2003), where the cloud-free irradiances are calculated by neglecting clouds in the radiation scheme.

2.1.2 Handling of surface albedo

The shortwave CRF is strongly affected by the assumed surface albedo. The ~~typically~~ potentially lower values of surface albedo in the cloud-free state (Walsh and Chapman, 1998) ~~should result in more positive~~ would result in a more positive estimate of shortwave $F_{\mathrm{net,cf}}$ ~~, and thus,~~ by the climatological approach compared to the instantaneous one using higher values of surface albedo under cloudy conditions. Thus, an increase of the cooling effect of clouds retrieved from the climatological approach relative to the instantaneous radiative ~~transfer based CRF , where a percent~~ transfer-based CRF has to be expected, whereby a percentage deviation of albedo can be related to the deviation of shortwave $F_{\mathrm{net,cf}}$.

For the instantaneous radiative transfer-based CRF, changes in surface albedo between the cloudy and cloud-free state have been neglected ~~so far~~ by the use of the ~~observed~~ prevailing (cloudy) albedo in the radiative transfer simulations (Intrieri et al., 2002; Shupe and Intrieri, 2004; Sedlar et al., 2011; Wang et al., 2018). ~~Miller et al. (2015) used~~ An exception is the study from Miller et al. (2015), where cloud-free observations of surface albedo are fitted linearly as a function of SZA to obtain cloud-

free albedo values during cloudy periods. This approach neglects the non-linear dependence of the albedo with SZA (Gardner and Sharp, 2010), the impact of snow grain size, and potential seasonal changes of cloud-free surface albedo indicated by the observed albedo shown in Miller et al. (2018), and thus, induces large uncertainties in the estimate of cloud-free shortwave net irradiance and may even distort the obtained seasonal cycle of CRF. The climatological approach from Long (2005) ~~tries to estimate~~ estimates the cloud-free surface albedo during cloudy periods based on ~~cloud-free observations~~ observations during cloud-free conditions, taking the prevailing SZA into account. However, it should be noted that for longer cloudy periods the cloudy-sky (observed) surface albedo is used in combination with downward cloud-free irradiance to represent the upward shortwave irradiance ~~,~~ because an extrapolation in changing albedo conditions caused by precipitation and melting events (changes in snow microphysical properties) is not possible. An application of the climatological approach is primarily limited by the high cloud fraction commonly observed in the Arctic (Shupe et al., 2011). It causes large uncertainties in the estimated cloud-free irradiance, as reported by Intrieri et al. (2002), preventing an application to long-term observations with reported high cloud fractions (e.g., Sedlar et al., 2011). Although the climatological approach will produce a more realistic estimate of CRF (especially longwave) with reduced uncertainties and representation of humidity changes (Dong et al., 2006), it remains unclear how representative a monthly average of cloud-free irradiance with a monthly averaged cloud fractions of often well above 90 % can be.~~By comparing the available studies, using different approaches to estimate the CRF, it becomes evident that the variety of strategies and the handling of physical processes involved in the CRF in the Arctic limits the comparability of the individual studies and our~~

The potential systematic differences in shortwave CRF estimates associated with the respective assumed surface albedo motivate to provide a quantitative measure of these differences as well as an improved solution for the albedo reference to enable a more harmonized understanding of CRF~~in the Arctic.~~ .

2.2 Definitions and process handling

~~In this study, we aim to~~ Below, we derive the radiative ~~transfer based~~ transfer-based instantaneous CRF. ~~However, we provide reasons and a solution for the derivation of shortwave CRF using a~~ Our approach is unique in that we use a continuous estimate of the cloud-free surface albedo of snow and ice obtained from concurrent observations in cloudy conditions.~~To assign processes related to single~~ , and in that we account for horizontal photon transport through using an areal-averaged surface albedo to compute the downward shortwave irradiances, as discussed below.

2.2.1 Longwave CRF

To distinguish between components of the surface CRF, Eq. 2 is separated in longwave and shortwave terms. The longwave ~~term reads:~~ component reads:

$$\Delta F_{\mathrm{lw}} = \left(F^{\downarrow}_{\mathrm{lw,all}} - F^{\uparrow}_{\mathrm{lw,all}}\right) - \left(F^{\downarrow}_{\mathrm{lw,cf}} - F^{\uparrow}_{\mathrm{lw,cf}}\right). \tag{3}$$

As was stated by Cox et al. (2015), the CRF definition refers to net irradiances, while the cloud radiative effect (CRE) ~~characterizes only~~ quantifies changes in the downward irradiance. By splitting the upward terms in Eq. 3 in a component

emitted by the surface with a temperature T_s and broadband surface emissivity ϵ_s of 0.99 (Warren, 1982) as well as a reflected residual of ~~$F_t^{\downarrow}$~~ $F_{lw}^{\downarrow}$:

$$-F_{lw,all}^{\uparrow} + F_{lw,cf}^{\uparrow} = -\epsilon_s \cdot \sigma \cdot T_s^4 - (1-\epsilon_s) \cdot F_{lw,all}^{\downarrow} + \epsilon_s \cdot \sigma \cdot T_s^4 + (1-\epsilon_s) \cdot F_{lw,cf}^{\downarrow}, \quad (4)$$

the upward term ~~:~~

~~$$-F_{lw,all}^{\uparrow} + F_{lw,cf}^{\uparrow} = -\epsilon_s \cdot \sigma \cdot T_s^4 - (1-\epsilon_s) \cdot F_{lw,all}^{\downarrow} + \epsilon_s \cdot \sigma \cdot T_s^4 + (1-\epsilon_s) \cdot F_{lw,cf}^{\downarrow},$$~~

reduces to:

$$-F_{lw,all}^{\uparrow} + F_{lw,cf}^{\uparrow} = (1-\epsilon_s) \cdot (F_{lw,cf}^{\downarrow} - F_{lw,all}^{\downarrow}). \quad (5)$$

This approach assumes ~~a~~ the same constant surface temperature in the cloudy and cloud-free state, and thus, represents the commonly defined instantaneous longwave CRF similar to ~~Shupe and Intrieri (2004); Sedlar et al. (2011); Miller et al. (2015) and~~ Shupe and Intrieri (2004), Sedlar et al. (2011), and Miller et al. (2015) and should be considered in the interpretation of the CRF values as discussed in the previous section. The essential input for radiative transfer simulations in the longwave wavelength range is the atmospheric temperature profile, the absorber gas profile and aerosol. Hence, the longwave instantaneous CRF ~~is independent on~~ becomes independent of the upward irradiance and reduces to:

$$\Delta F_{lw} = F_{lw,all}^{\downarrow} - F_{lw,cf}^{\downarrow} + (1-\epsilon_s) \cdot (F_{lw,cf}^{\downarrow} - F_{lw,all}^{\downarrow}). \quad (6)$$

2.2.2 Shortwave CRF

The shortwave component of the CRF is given by:

$$\Delta F_{sw} = \left(F_{sw,all}^{\downarrow} - F_{sw,all}^{\uparrow}\right) - \left(F_{sw,cf}^{\downarrow} - F_{sw,cf}^{\uparrow}\right). \quad (7)$$

The surface albedo α ~~as a~~ is defined as the ratio of $F_{sw}^{\uparrow}$ and $F_{sw}^{\downarrow}$ ~~measured during low-level flights is introduced into Eq. 7, which leads to the~~. To account for surface albedo changes due to different illumination conditions (cloudy, cloud-free) and cloud optical thickness (Warren, 1982), the surface albedo is decomposed into an albedo observed in cloudy conditions (α_{all}) and an albedo, which continuously represents the cloud-free state (α_{cf}). Thus, the instantaneous shortwave CRF definition ~~:~~ reads:

$$\Delta F_{sw} = \left(F_{sw,all}^{\downarrow} - \alpha_{all} \cdot F_{sw,all}^{\downarrow}\right) - \left(F_{sw,cf}^{\downarrow} - \alpha_{cf} \cdot F_{sw,cf}^{\downarrow}\right). \quad (8)$$

~~The~~

Another relevant parameter is the radiative transfer simulated downward shortwave irradiance at the surface in cloud-free conditions ($F_{sw,cf}^{\downarrow}$), which is modulated by ~~the atmospheric profile~~ atmospheric parameters, but also by the surface albedo. For highly reflective surface types ~~like snow~~such as snow, the upward irradiance is significantly higher compared to values obtained

over mostly absorbing surfaces like ocean water. ~~A part of this~~ Partly the upward irradiance is scattered back towards the surface ~~(often referred to as multiple scattering), and thus, contributes to~~ contributing to the downward irradiance. Consequently, the multiple scattering between surface and atmosphere causes an increase of downward irradiance over snow and ice compared to open ocean. Photons reflected from a bright ~~surfaces like an ice flow might scatter~~ surface might be scattered back to the surface increasing the downward radiation over dark areas ~~like~~ in surrounding ocean water. This might typically happen in the vicinity of the MIZ or in case of leads. For airborne observations in the MIZ ~~, characterized by strong variability in surface albedo due to the variable sea ice cover,~~ as well as ground based measurements in heterogeneous terrain, this ~~, often referred to as, horizontal photon transport due to multiple scattering from the surrounding area to the actual point of observation~~ effect is not negligible for ~~the estimate of~~ $F^{\downarrow}_{\mathrm{sw}}$ (Ricchiazzi and Gautier, 1998; Kreuter et al., 2014).

To address this problem, the downward irradiance for the cloud-free conditions in regions with heterogeneous surface albedo ~~fields~~ needs to be simulated with an ~~areal averaged~~ areal-averaged albedo α_{ar}, also called effective albedo (Weihs et al., 2001; Wendisch et al., 2004). For example, a local surface albedo over a small lead embedded in homogeneous sea ice is not representative for the ~~areal average surface albedo, determining the scattering processes in cloud-free conditions. To illustrate this approach,~~ areal-averaged surface albedo. To complete the formulation of the shortwave CRF used in this study we modify Eq. 8 to:

$$\Delta F_{\mathrm{sw}} = \left(F^{\downarrow}_{\mathrm{sw,all}} - \alpha_{\mathrm{all}} \cdot F^{\downarrow}_{\mathrm{sw,all}}\right) - \left(F^{\downarrow}_{\mathrm{sw,cf}}\Big|_{\alpha_{\mathrm{ar}}} - \alpha_{\mathrm{cf}} \cdot F^{\downarrow}_{\mathrm{sw,cf}}\Big|_{\alpha_{\mathrm{ar}}}\right). \tag{9}$$

where $F^{\downarrow}_{\mathrm{sw,cf}}\Big|_{\alpha_{\mathrm{ar}}}$ represents the downward shortwave irradiance at the surface simulated with the ~~areal average~~ areal-averaged albedo in cloud-free conditions.~~Besides affecting the $F^{\downarrow}_{\mathrm{sw}}$, the surface albedo α in Eq. ?? changes for different illumination conditions (cloudy, cloud-free) and cloud optical thickness Warren (1982). Thus, to complete the formulation of the shortwave CRF used in this study,~~

In section 4, the impact of clouds on α_{cf} and its influence on the estimate of CRF is analyzed using radiative transfer simulations. In section 5.1 the impact of horizontal photon transport on $F^{\downarrow}_{\mathrm{sw,cf}}\Big|_{\alpha_{\mathrm{ar}}}$ and the CRF is quantified by illustrative ACLOUD observations.

3 Observations and modeling

3.1 Airborne measurements and instrumentation

The cloudy atmospheric boundary layer in the MIZ northwest of Svalbard was studied using the research aircraft Polar 5 and Polar 6 from the Alfred Wegener Institute (AWI) during the ACLOUD campaign performed in spring between 23 May and 26 June 2017 (Wendisch et al., 2019). Parts of the flights were dedicated to characterize the near-surface radiative energy budget below ABL clouds. 16 hours of data measured below clouds (if present) at an altitude less than 250 m (average 80 m) covering a distance of 3700 km were collected. The sea ice concentration observed along the low-level flights by instruments mounted on the aircraft is displayed in Fig. 1, together with a Moderate Resolution Imaging Spectroradiometer (MODIS)

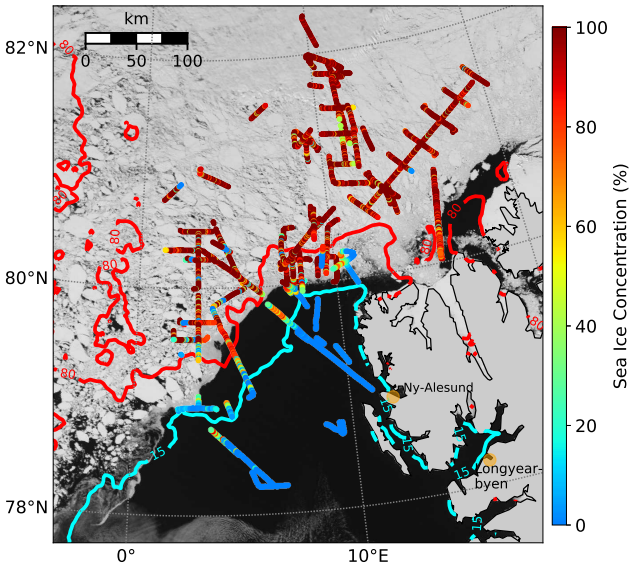

Figure 1. MODIS satellite image on 1 June 2017, representing the typical sea ice distribution during the ACLOUD campaign. All low-level flight sections during the ACLOUD campaign are indicated with the sea ice fraction derived from airborne observations. Red (80 %) and light-blue (15 %) contours indicate the campaign average sea ice fraction from daily satellite-based sea ice data (Spreen et al., 2008).

satellite image. During the ACLOUD campaign, the ~~local surface albedo has to be separated in a cloudy albedo (α_{all}) and an albedo, which continuously represents the~~ location of the MIZ, indicated by the contour lines of average sea ice fraction (I_{f}), was almost stationary (Knudsen et al., 2018). The sea ice was more compact (higher concentration) north of 81° N geographic latitude, and rather heterogeneous towards the west and the open ocean. The majority of flights was conducted over the MIZ with 66 % over areas with high ice concentration ($I_{\mathrm{f}} > 80\,\%$) and 17 % over the region with moderate ice concentration ($80\,\% > I_{\mathrm{f}} > 15\,\%$) and 17 % over the more or less open ocean ($I_{\mathrm{f}} < 15\,\%$). As the dataset is merged from different flights covering about six weeks, it comprises various sea ice characteristics and synoptic situations (Knudsen et al., 2018). The data should be considered as a snapshot of the late spring conditions in this region.

The instrumentation of Polar 5 and Polar 6 during the ACLOUD campaign is described by Wendisch et al. (2019) and by Ehrlich et al. (2019b). In this paper, shortwave and longwave, upward and downward broadband irradiance measurements are analyzed. The data were collected with a frequency of 20 Hz using two sets of pyranometers (0.2-3.6 µm) and pyrgeometers (4.5-42 µm) (Stapf et al., 2019a). From these irradiance data the net irradiance and surface albedo were derived. The processing of the pyranometer and pyrgeometer data is detailed in Ehrlich et al. (2019b). The surface brightness temperature was determined by a Kelvin Infrared Radiation Thermometer (KT–19) (Stapf et al., 2019a). The ice fraction I_{f} along the flight track was estimated from measurements of a digital camera equipped with a hemispheric lens. The geometrically calibrated images were obtained with a sampling frequency of 6 s; from the images the cosine-weighted sea ice concentration was calculated (Jäkel et al., 2019). The local atmospheric thermodynamic state, including air temperature and relative humidity, was determined

by dropsondes (Ehrlich et al., 2019a) and aircraft in situ observations (Hartmann et al., 2019) during ascents and descents in the vicinity of the low-level flight sections.

3.2 Radiative transfer simulations

The radiative transfer simulations for the cloud-free ~~state α_{cf}. As a result Eq. ?? reads:~~

$$\Delta F_{\mathrm{sw}} = \left(F^{\downarrow}_{\mathrm{sw,all}} - \alpha_{\mathrm{all}} \cdot F^{\downarrow}_{\mathrm{sw,all}}\right) - \left(F^{\downarrow}_{\mathrm{sw,cf}}\Big|_{\alpha_{\mathrm{ar}}} - \alpha_{\mathrm{cf}} \cdot F^{\downarrow}_{\mathrm{sw,cf}}\Big|_{\alpha_{\mathrm{ar}}}\right).$$

~~In the following sections, these two key components (the impact of horizontal photon transport $F^{\downarrow}_{\mathrm{sw,cf}}\big|_{\alpha_{\mathrm{ar}}}$ (section 5.1)and the impact of clouds on α_{cf} of the CRF estimate (section ??)) are analysed using synthetic~~ conditions were performed with the libRadtran package (Emde et al., 2016) using the one-dimensional, plane-parallel discrete ordinate radiative transfer solver DISORT (Stamnes et al., 1988), and the molecular absorption parameterization from Kato et al. (1999) for the shortwave spectral range (0.28–4 µm), and from Gasteiger et al. (2014) for the longwave wavelengths range (4–100 µm). The aerosol particle optical thickness was neglected in the simulations because the full column aerosol information was not available for low-level flights in cloudy conditions. Therefore, the estimated CRF needs to be considered as direct aerosol plus cloud radiative forcing.

The atmospheric state, required as input for the radiative transfer simulations, was based on in situ measurements of temperature and relative humidity on board of both aircraft and, if available, dropsonde measurements from the Polar 5 aircraft. For the thermodynamic state above the flight altitude of the aircraft, the in situ observations were merged with radiosoundings from Ny-Ålesund (Svalbard) (Maturilli, 2017a, b) and onboard Polarstern (Schmithüsen, 2017), which were partly spatially and temporally separated from the airborne observations by several hundred kilometres and up to three hours. The temperature profile below the lowest flight altitude was linearly interpolated to the surface brightness temperature observed by the KT19. For cloudy conditions radiative transfer simulations ~~and illustrative ACLOUD observations, in order to quantify their separate impact on the CRF in the Arctic.~~ (assuming a surface emissivity of 0.99, Hori et al., 2006) of the observed atmospheric profiles indicate that neglecting an atmospheric correction for cloudy conditions is justified and the brightness temperature of the KT19 can be related to the surface temperature causing uncertainties below ±0.2 K. During cloud-free conditions a correction of 0.5 K has been added to the brightness temperature (average value obtained from radiative transfer simulations) to compensate for atmospheric and surface emissivity effects. The impact of flight altitude (average 80 m) can be neglected and potential surface temperature uncertainties hardly affect the downward irradiance simulated in flight altitude. The sub-Arctic summer profile (Anderson et al., 1986) was used to complete the profiles including gas concentrations up to 120 km altitude. Daily ozone concentrations in the flight region of ACLOUD were considered and obtained from http://exp-studies.tor.ec.gc.ca/cgi-bin/selectMap. The high vertical resolution of the in situ observations was reduced for the radiative transfer simulations to 30 m below 1000 m and stepwise increases to 5 km at 120 km altitude. The surface albedo was obtained from upward and downward looking pyranometers and a method described in section 5.2.

Spectral surface albedo values for the sensitivity study in section 4 were simulated using the spectral Two-streAm Radiative TransfEr in Snow model (TARTES) (Libois et al., 2013). 3D radiative transfer simulations for the albedo smoothing kernels

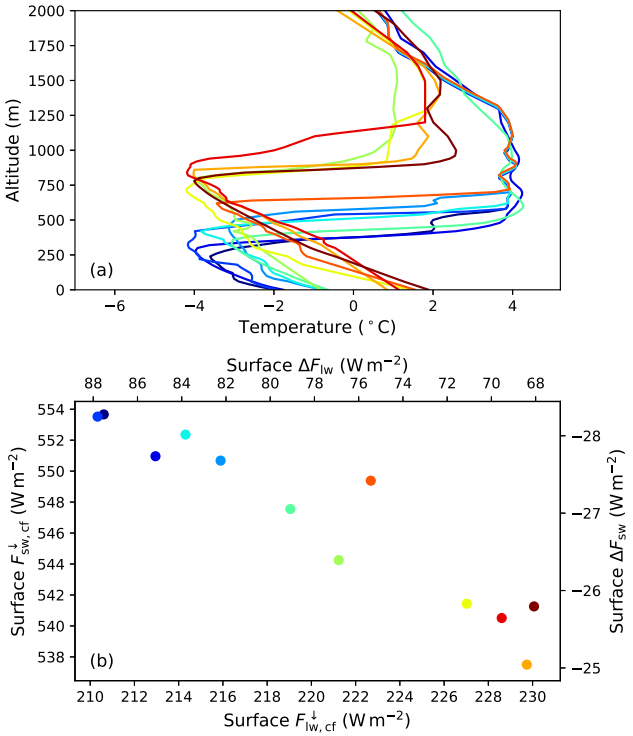

Figure 2. (a) Temperature profiles observed during the warm air intrusion on 2 June 2017. The profiles are obtained from dropsonde and in situ measurements (merged with radiosoundings) and are color-coded by the air temperature in the lowest 200 m. (b) Correlation between simulated cloud-free $F^{\downarrow}_{sw}$ and $F^{\downarrow}_{lw}$ assuming the observed atmospheric profiles from (a) (same color code). The second x and y axis shows the expected longwave/shortwave CRF at the surface by assuming a constant $F^{\downarrow}_{sw,all}$ (412 W m^{-2}) and $F^{\downarrow}_{lw,all}$ (298 W m^{-2}) based on observations. For a better comparability, the surface albedo and the SZA was fixed in the simulations to 0.8 and 60°, respectively.

applied in section 5.1 and the Appendix A were performed with the open-source Monte Carlo Atmospheric Radiative Transfer Simulator (MCARaTS) (Iwabuchi, 2006; Iwabuchi and Kobayashi, 2008).

3.3 Necessity of a local thermodynamic profile for the estimate of CRF

3.4 ~~Impact of local thermodynamic atmospheric state~~

In the MIZ, the thermodynamic state of the atmosphere changes within short distances due to the influence of the surface on the airmass (warm air moving north ~~over~~ towards cold sea ice, cold air moving south ~~over~~ towards warm open ocean) (e.g., Lampert et al., 2012). As ~~was~~ shown by Tjernström et al. (2015, 2019)~~such events might~~ , such events significantly impact the local energy budget along the trajectory. As an example of ~~temperature profiles being influence by~~ the influence of surface properties and large scale processes ~~, the spatial variability of air temperature profiles~~on temperature profiles, drop sonde and in situ data measured on 2 June 2017 by ~~the aircraft instruments (~~instruments installed on Polar 6 ~~) and dropsondes is illustrated~~

are shown in Fig. 2a. The ~~synoptical~~ synoptic situation during this flight (west of Svalbard) was characterized by southbound warm air advection with optically thick clouds moving from the open ocean over the MIZ. The consecutive in situ profiles illustrate the changes in inversion height along the flight leg, which changed from roughly 800 m over the ocean to 250 m over the sea ice within 50 to 100 km. The relative humidity (not shown here) changed accordingly.~~For the shown~~

Using these profiles, radiative transfer simulations are performed to calculate $F^{\downarrow}_{\mathrm{sw,cf}}$ and $F^{\downarrow}_{\mathrm{lw,cf}}$~~for the cloud-free reference case~~. The surface albedo and SZA is fixed for this sensitivity study to 0.8 and 60° respectively, similar to the observed conditions over sea ice during that flight~~, in order to avoid any~~ . Therefore, the results only show the impact of changing thermodynamics, but not the effects induced by ~~changing~~ the observed changes in SZA or surface albedo. Fig. 2b shows the simulated downward irradiance and corresponding values of the shortwave and longwave CRF. While longwave irradiance increases with increasing humidity and temperature (enhanced emission), the shortwave irradiance decreases (enhanced scattering and absorption). The CRF for each ~~case~~ atmospheric profile is estimated using the average observed $F^{\downarrow}_{\mathrm{sw,all}}$ and $F^{\downarrow}_{\mathrm{lw,all}}$ during the low-level ~~section~~ flight legs observed on 2 June 2017. The results show a strong variability in ΔF induced by changes in the thermodynamic structure. The relative deviations range up to 29 % for the longwave and 11 % for the shortwave CRF, which highlights ~~that neglecting~~ the need to consider changes of the atmospheric thermodynamic state within a few kilometers ~~can cause significant errors in the retrieved~~ to derive the CRF. Especially for airmass transformation like warm air intrusions and cold air outbreaks in the Arctic (Pithan et al., 2018), this is a relevant issue~~, and requires a precise representation of airmass transformations by models or local in situ observations along the trajectory. Another aspect regarding the thermodynamic state of the atmosphere is the impact of the average aircraft flight altitude (here 80) on the estimate of CRF. The $F^{\downarrow}_{\mathrm{lw,cf}}$ is simulated for local flight altitude and not exactly for the surface. Due to the fact that the vertical gradient $dF^{\downarrow}_{\mathrm{lw}}/dz$ and $dF^{\uparrow}_{\mathrm{lw}}/dz$ below clouds remains almost the same with or without a cloud in the radiative transfer simulations (for atmospheric profiles as observed during ACLOUD), the observed CRF in flight altitude can be related to surface CRF values causing uncertainties below ±5 . For an interpretation of single longwave irradiance directions and a comparison to surface observations (both not shown in this study), changes due to prevailing near-surface temperature profile have to be expected.~~

3.4 ~~Impact of areal versus local surface albedo~~

~~In Fig. 1 the variability of the observed sea ice fraction I_{f} can directly be related to the variability in the surface albedo distributions in the MIZ and will influence the observed field of downward shortwave irradiance. For the observations carried out on 23 May 2017, the measured broadband surface albedo along the flight track is shown in Fig. 7a. The low-level section started in the MIZ over large ice floes and small leads and ended over the open ocean in vicinity of the ice edge with occasionally scattered sea ice floe fields. Leads with the size of a few tens of meters up to a few kilometers caused a highly variable local surface albedo.Time series (covered distance) of measured broadband surface albedo (black) (a) and simulated $F^{\downarrow}_{\mathrm{sw,cf}}$ (b) along the low-level flight track during the 23 May 2017. The red line in (a) shows the areal averaged albedo using the kernel embedded in (b). (b) The gray area shows the potential variability of $F^{\downarrow}_{\mathrm{sw,cf}}$ due to surface albedo changes. The black and red scatter shows the $F^{\downarrow}_{\mathrm{sw,cf}}\big|_{\alpha}$ and $F^{\downarrow}_{\mathrm{sw,cf}}\big|_{\alpha_{\mathrm{ar}}}$ respectively. (c) Difference in shortwave CRF estimate between $\Delta F_{\mathrm{sw}}(\alpha_{\mathrm{ar}})$ and $\Delta F_{\mathrm{sw}}(\alpha)$. In Fig. 7b the simulated $F^{\downarrow}_{\mathrm{sw,cf}}$ using the observed 20 surface albedo illustrates the problems related with strong~~

albedo fluctuations. The simulated $F^{\downarrow}_{\mathrm{sw,cf}}$ changes on small horizontal scales by up to 35 (SZA average: 59.2°). However, due to horizontal photon transport from surrounding ice fields, in reality the changes in $F^{\downarrow}_{\mathrm{sw,cf}}$ are less pronounced. The quantitative impact of multiple scattering on $F^{\downarrow}_{\mathrm{sw,cf}}$ is indicated by the gray shaded area in Fig. 7b with a maximum contribution of almost 40 (relative to open ocean). Therefore, the downward irradiance for the cloud-free conditions, required for Eq. 9, needs to be simulated with an appropriate areal averaged albedo representing the multiple scattering contribution from the surrounding albedo fields.To estimate a required filter shape and width to obtain an areal averaged albedo, 3D radiative transfer simulations of a typical scenario are performed (not shown here), where leads of different sizes are embedded in homogeneous sea ice similar to the study from Podgorny et al. (2018). The simulated irradiance of the 3D model output in the vicinity of the leads is reproduced by 1D simulations by applying the filter embedded in Fig. 7b to the theoretically observed albedo and by using the obtained areal averaged albedo for the 1D model simulations to continuously estimate the $F^{\downarrow}_{\mathrm{sw,cf}}$. The appropriate weighting of near-field and far-field albedo is applied by kernel k defined by a Laplace-distribution:

$$k(x,\mu,\gamma) = \frac{1}{2\gamma}\left(-\frac{|x-\mu|}{\gamma}\right),$$

with γ.

4 Modeling the surface albedo-cloud interaction

4.1 Impact of clouds on surface albedo

The effect of 5 , the median μ and a scale x of 30 . This rather large filter width indicates that small leads below 1embedded in homogeneous sea ice show a minor impact on $F^{\downarrow}_{\mathrm{sw}}$ in cloud-free conditions.The resulting areal averaged albedo is shown in Fig. 7a, together with the simulated $F^{\downarrow}_{\mathrm{sw,cf}}\big|_{\alpha_{\mathrm{ar}}}$ (Fig. 7b), which follows the large scale trends of surface albedo but mitigates small scale fluctuations. Neglecting these effects would result in uncertainties of the local shortwave CRF estimate, as shown in Fig. 7c. On average, the effect for flight section in Fig. 7 is of minor importance (average -1.9), because under- and overestimation of shortwave CRF cancel in this specific example, similar to results from Benner et al. (2001). Nevertheless, on a local scale it should be highlighted that due to horizontal photon transport the $F^{\downarrow}_{\mathrm{sw,cf}}\big|_{\alpha_{\mathrm{ar}}}$ is up to 28 larger above leads compared to the $F^{\downarrow}_{\mathrm{sw,cf}}\big|_{\alpha}$. The difference in the derived CRF reaches values between -25 over open water embedded in homogeneous sea ice, where the $F^{\downarrow}_{\mathrm{sw,cf}}$ is underestimated by applying the local albedo, and +6 above scattered ice floe fields in the ocean with an overestimation of $F^{\downarrow}_{\mathrm{sw,cf}}$. Hence, the uncertainties and artificial fluctuations in CRF are limited by applying the smoothed albedo in the $F^{\downarrow}_{\mathrm{sw,cf}}$ simulations. This enables a more reliable estimate of the CRF in the heterogeneous MIZ and over the specific surface types, taking into account that the complexity of surface albedo fields in the MIZ can only be insufficiently represented by this simplified approach to estimate the areal averaged albedo.Histogram of shortwave, longwave and total ΔF derived during the cloud-free ACLOUD flight on 25 June 2017. Statistics are given in the gray box (mean $\varnothing$, standard deviation σ).

4.1.1 Uncertainty estimate in cloud-free conditions

During ACLOUD a flight in cloud-free conditions on 25 June 2017 can be used for a comparison between measured and simulated irradiances to estimate the accuracy of this dataset. The difference between observed and simulated $F_{\mathrm{cf}}^{\downarrow}$ for the low level flights of both aircraft (2.1 hours of data) is 5.7 ± 7.1 (1.1 %) in the shortwave and 0.41 ± 1.45 (0.2 %) in the longwave irradiance. The histograms of the CRF for that day are shown in Fig. 9. The mean values of the entire flight section is 2.15 in the shortwave and 0.41 in the longwave. The slightly positive CRF might be caused by the upper air sounding approximately 300 km in the south of the flight track or the aerosol conditions (aerosol optical thickness was set to zero in the simulation). In addition to the measurement uncertainties of the used broadband radiometer (<3 %, (Ehrlich et al., 2019b)), the radiative transfer modelling can induce a bias (<2 %) in the shortwave wavelength ranges (Randles et al., 2013). Due to the absence of cloud-free conditions during other low-level flights of the ACLOUD campaign this comparison can be considered as a rough estimate of potential uncertainties during the whole ACLOUD campaign.

4.2 Impact of clouds on the surface albedo

The effect of clouds on the broadband surface albedo, implemented in Eq. 9, is analysed by a set of spectral albedos albedo spectra of three sea ice types common in the Arctic for different seasons. Different snow packs with a density of 300 $\mathrm{kg\,m^{-2}}$ are specified with various values of and variable snow geometric thickness and specific surface area (SSA, a measure of snow grain size) (Gardner and Sharp, 2010) were defined, and located above a layer representing bare sea ice with a wavelength constant wavelength-constant broadband albedo of 0.5. Fresh cold and dry snow (SSA = 80 $\mathrm{m^2\,kg^{-1}}$, 20 cm thick) represents early to late spring conditions, melting snow (SSA = 5 $\mathrm{m^2\,kg^{-1}}$, 20 cm thick) the melting season in late spring early summer, and thin melting snow/white ice (SSA = 5 $\mathrm{m^2\,kg^{-1}}$, 1 cm thick) summer conditions, before the melt pond formation. The spectral albedo for each type is simulated with the TARTES model for 65° SZA; the respective results are shown in Fig. 3 (solid lines) together with simulated downward irradiances from the atmospheric radiative transfer simulations using the corresponding downward irradiances simulated with libRadtran (shaded spectra).The general

The impact of snow properties on the spectral surface albedo is characterized by stronger absorption at longer wavelengths the fact that with decreasing SSA (increasing effective grain size) and can be seen the absorption at longer wavelengths increases (Warren, 1982; Gardner and Sharp, 2010). It becomes obvious by comparing the albedo of fresh and melting snow in Fig. 3. A Thus, a decreasing SSA amplifies the contrast between shorter and longer wavelength. A wavelengths. In contrast, a thinning of the snow layer or impurities in snow enhance the absorption mainly in the shorter visible wavelength range, as illustrated by the albedo of melting snow in comparison to that of white ice.

Two processes influencing the broadband snow albedo are related to the transition from cloud-free to cloudy atmospheric conditions. In an overcast atmosphere with clouds of sufficient optical thickness, mainly diffuse radiation illuminates the surface as compared to cloud-free conditions, when the direct shortwave radiation dominates (Gardner and Sharp, 2010). In the Arctic, large values of SZA (> 50°) are common. In overcast conditions, scattering processes in clouds effectively decrease the averaged incoming (effective) angle of the mainly diffuse irradiance to approximately 50° above snow (Warren, 1982).

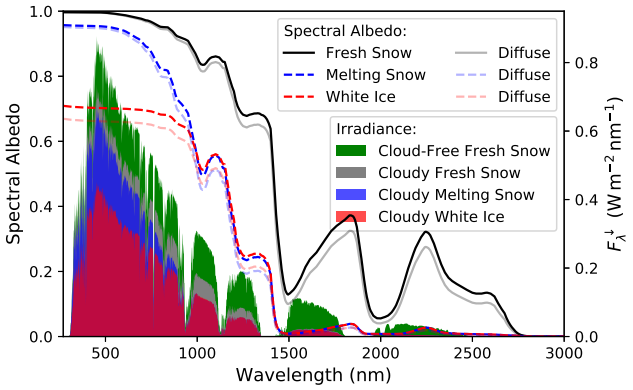

Figure 3. Simulated spectral snow albedo of three seasonal sea ice types ~~for~~ generated using different SSA and snow thickness values (specified in the main text) above sea ice with spectrally neutral albedo of 0.5. Non-attenuated lines show the albedo of the cloud-free situations (SZA of 65°), attenuated lines (transparent colors) represent the albedo for overcast/diffuse conditions (color-related). The downward irradiance (right y-axis) simulated for these cases are shown by the shaded areas. Green shows the cloud-free spectra over fresh snow, gray, blue and red under cloudy conditions (LWP of 80 g m^{-2}) for the surface albedo related by the colors.

With decreasing so-called effective SZA, the penetration depths of photons into the snow and ice surface increases, enhancing the probability of absorption, and thus, decrease the overall broadband surface albedo (Warren, 1982). In Fig. 3 this effect is illustrated by the attenuated lines (transparent colors) representing the respective diffuse albedo values. Compared to the surface albedo of fresh snow in cloud-free atmospheric conditions (black line) the change of effective SZA (in this example from 65° to approximately 50° SZA) causes a lower spectral surface albedo (attenuated black line) in the non-visible wavelength range, while the highly reflective visible wavelengths are not affected. Thus, for this surface type only a small impact on the actual broadband albedo can be expected, because for the majority of the related downward shortwave irradiance (e.g. grey shaded area in Fig. 3) the albedo remains high. However, for surface types with a spectral albedo characterized by stronger absorption in the visible wavelength range (albedo of white ice, red dashed line in Fig. 3), also stronger changes between direct-dominated and diffuse ~~broadband albedo are expected (attenuated~~ albedo (attenuated dashed red line) ~~.~~and thus also the broadband albedo are expected.

Besides the ~~changing effective SZA~~ cloud-induced changes of the effective SZA discussed above, clouds reduce the incident irradiance by attenuating especially in the near-infrared wavelength range (Grenfell and Perovich, 2008)~~, which~~ . This can be seen in Fig. 3 by comparing the green and gray shaded spectrum representing cloud-free ~~,~~and cloudy conditions with a liquid water path (LWP) of 80 g m^{-2}, respectively. In this example, the presence of the cloud reduces the downward irradiance by 18 % at a wavelength of 500 nm and 78 % at 1600 nm. With increasing cloud optical thickness the spectral slope of downward irradiance is imprinted in the surface spectra. As the spectral albedo of ice and snow is higher for shorter wavelengths (e.g. black line in Fig. 3) and the downward irradiance spectra ~~is~~ are shifted to shorter ~~wavelength~~wavelengths in the presence of clouds, the wavelength integrated (broadband) albedo will increase. This effect becomes stronger the more pronounced

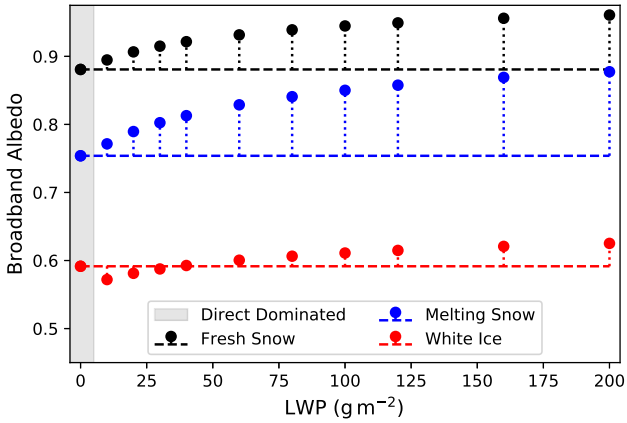

Figure 4. Broadband albedo integrated from simulated up- and downward spectral irradiance as a function of cloud LWP (r_{eff} of 8 µm) using the color-related ~~spectral albedos~~ albedo spectra of Fig 3 and a SZA of 65°. The approximate area of direct dominated ~~/ cloud free~~ radiation is indicated by the gray shading~~(SZA of 65°)~~. The horizontal dashed line indicates the cloud-free albedo as a reference.

the slope between visible and near-infrared wavelength becomes, which can be induced by two processes: either stronger absorption by clouds due to a higher LWP, or by the underlying surface albedo with decreasing near-infrared albedo. The latter is controlled by decreasing SSA (transition from fresh to melting snow), resulting in a reduced near-infrared reflection of the surface (compare black and dashed blue lines in Fig. 3), which indirectly affects $F_{\mathrm{sw}}^{\downarrow}$ by a reduced multiple scattering between surface and clouds in this wavelength range (compare grey and blue shaded spectra). However, for the spectral albedo of white ice (dashed red line) the slope in the $F_{\mathrm{sw}}^{\downarrow}$ ~~spectra~~ spectrum (red shaded) is less pronounced than in the other cases, and a weaker increase of broadband albedo is expected for increasing LWP.

For all three surface albedo types shown in Fig. 3, the effect of clouds (as a function of LWP) on the broadband surface albedo ~~,~~ is presented in Fig. 4~~for a SZA of 65°. An effective cloud droplet radius (r_{eff}) of 8 is used. The gray area indicates the direct-dominated radiation in cloud-free conditions; dashed lines represent the cloud-free albedo value as a reference.~~ For the different surface types, a significant change of up to 12 % relative to the individual cloud-free values of surface albedo can be found with increasing cloud optical thickness, which is modulated by the interaction of surface and cloud radiative properties. In general, the lower the ratio of spectral surface albedo between shorter and longer wavelengths is, the stronger is the increase of broadband albedo with increasing LWP~~, as shown for the black and blue scatter in Fig. 4 representing fresh and melting snow, respectively.~~ . Spectral absorption of the surface in shorter wavelengths ~~strongly~~ decreases the broadband surface albedo, but it will also alter the behaviour with increasing LWP (Fig. 4, red). For low LWP values, the broadband surface albedo is lower compared to cloud-free conditions due to a significant lower spectral diffuse albedo (dashed red and attenuated dashed red line in Fig. 3) at shorter wavelengths. However, with increasing LWP the weighting effect in transmitted $F_{\mathrm{sw}}^{\downarrow}$ to shorter wavelength compensates/dominates and, as a consequence, it increases the broadband surface albedo compared to cloud-free conditions.

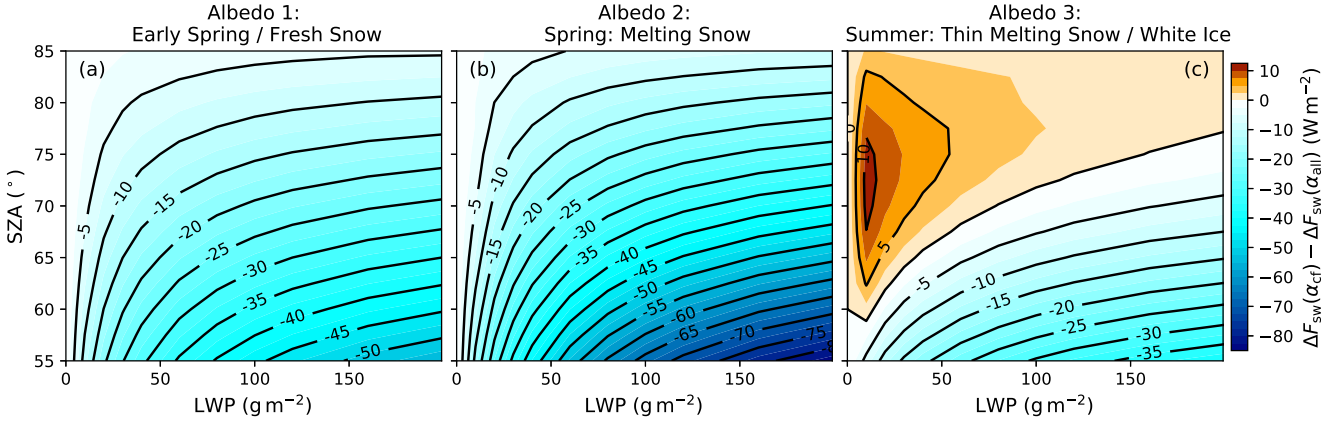

Figure 5. Bias of the shortwave CRF ($\Delta F_{\mathrm{sw}}(\alpha_{\mathrm{cf}}) - \Delta F_{\mathrm{sw}}(\alpha_{\mathrm{all}})$) caused by neglecting the change between observed cloudy and cloud-free surface albedo as a function of cloud LWP ($r_{\mathrm{eff}} = 8\,\mu\mathrm{m}$) and SZA. The three albedo types from Fig. 3 have been assumed, (a) fresh snow representative for early spring, (b) melting snow during late spring, and (c) thin melting snow/white ice found in early summer. Negative (bluish) values indicate a stronger shortwave cooling effect for $\Delta F_{\mathrm{sw}}(\alpha_{\mathrm{cf}})$. Changes in direct/diffuse radiation due to SZA are taken into account.

4.1.1 ~~Surface albedo-cloud interaction and CRF~~

~~In calculations of the instantaneous CRF based on radiative transfer, the observed surface albedo below clouds serves as a reference for the simulations of $F_{\mathrm{net,cf}}$ and calculation of ΔF_{sw}. Also weather and climate models, where the change of the broadband albedo with increasing LWP is not, or only poorly, parameterized, may have a bias in the estimated CRF as well as in the $F_{\mathrm{net,cf}}$ in cloudy conditions.~~

4.2 Impact on shortwave CRF

To estimate the significance of the surface albedo-cloud interaction on CRF, radiative transfer simulations are used~~to calculate the shortwave CRF~~, either assuming the correct cloud-free surface albedo as a reference, or the prevailing ~~cloudy albedo~~ surface albedo in cloudy conditions, as shown in Fig 4. The difference in CRF ($\Delta F_{\mathrm{sw}}(\alpha_{\mathrm{cf}}) - \Delta F_{\mathrm{sw}}(\alpha_{\mathrm{all}})$) between both approaches ~~,~~ and thus, an underestimate of the shortwave cooling effect if the cloudy albedo is used, is is shown in Fig. 5 as a function of SZA and LWP~~($r_{\mathrm{eff}} = 8$).Negative (bluish) values indicate a stronger shortwave cooling effect for $\Delta F_{\mathrm{sw}}(\alpha_{\mathrm{cf}})$. The simulations are performed for all three sea ice types in Fig. 3 and changes in direct/diffuse radiation due to SZA are taken into account.~~.

In case of snow surfaces, influenced by the SSA (Fig. 5a and b), the cooling effect of clouds on the surface is underestimated (~~blue~~ bluish colors), if the cloudy albedo (α_{all}) is used to derive the shortwave CRF. In general, the lower the SZA and the higher the LWP are, the stronger the underestimation of the cooling effect becomes. Furthermore, the coarser the snow grains (melting snow) the stronger the underestimation. In contrast, during summer and for thin melting snow or white ice (Fig. 5c), the cooling effect is overestimated for low sun and optically thin clouds, if the apparent cloudy albedo is used for ΔF_{sw}, and

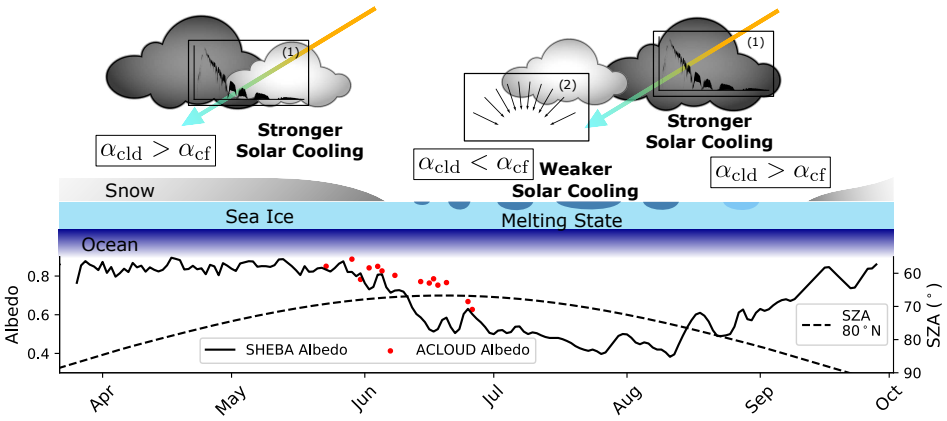

Figure 6. ~~Hypothetical~~ Conceptual scheme of the seasonal cycle of surface albedo-cloud interaction related modification of shortwave CRF causing a stronger or weaker cooling relative to $\Delta F_{sw}(\alpha_{all})$. Dominant processes influencing the transition from cloudy (~~eld~~α_{cld}) to cloud-free surface albedo (α_{cf}) in the specific season are represented by the icons (1) (weighting of downward irradiance to shorter wavelength with increasing LWP) and (2) (transition from direct to diffuse radiative transfer). The seasonal cycle of surface broadband albedo is shown by SHEBA observations (200 m albedo line). Averaged ACLOUD observations for homogeneous sea ice ($I_f > 95\,\%$) are shown in red scatter points. Computed daily averaged SZA for 80° N in dashed black.

shifts towards the underestimation for optically thick clouds and/or lower SZA.~~The values of underestimation/overestimation indicate that the~~

The surface albedo-cloud interaction significantly ~~impact~~ impacts the estimate of shortwave CRF and the obtained values from the different approaches in the available CRF studies in the Arctic. Especially for clouds over snow, the cooling effect of clouds is considerably larger ~~.~~ when cloud-related changes in surface albedo are considered. Also for climate models with simple albedo parameterizations, for example fixed broadband albedo values for certain surface types, the results from Fig. 5 can be interpreted as a potential bias in the shortwave REB and CRF depending on the cloud optical thickness. Due to the dependence on specific spectral surface albedo types, a seasonal dependence of this surface albedo-cloud interaction, and thus, the shortwave CRF, is indicated.

4.3 Seasonal cycle of shortwave CRF

In Fig. 6 a ~~hypothetical~~ conceptual scheme of the modified seasonal cycle of CRF due to the surface albedo-cloud interaction ~~,~~ is proposed. The time series of surface albedo as observed during the Surface Heat Budget of the Arctic Ocean (SHEBA) campaign (Uttal et al., 2002) (data from Roode and Bretherton, 2007) is shown, to illustrate the seasonal transition as reported by Perovich et al. (2002)~~, together with a daily averaged SZA for 80° N~~. During spring, early summer~~and autumn~~ , and autumn, surface albedo values related to snow on sea ice are found. The results from Fig. 5 indicate that the cloud generated shift of transmitted irradiance towards shorter wavelength (process 1 in Fig. 6) is dominant in these situations~~and clouds~~ /seasons and clouds actually induce a stronger cooling effect on the surface, relative to $\Delta F_{sw}(\alpha_{all})$. With the beginning of the melting

season, the change between diffuse and direct albedo will dominate (process 2) for ~~optical~~ optically thin clouds and high SZA, potentially reducing the clouds' cooling effect on the surface ~~in dependence of~~ depending on the conditions. In this period the onset of melting (rapidly decreasing albedo), the melt pond fraction, and the SZA (dashed black line in Fig. 6) together with the cloud optical thickness would critically ~~influences~~ influence the sign of this modification. However, as was reported by Walsh and Chapman (1998), for regions where ~~even in summer~~ snow or bare sea ice is found ~~, all year long~~ even in summer, a lower albedo in cloud-free conditions, and thus, a stronger cooling effects of clouds can be expected all year long. Though, conclusions about the ~~annual~~ annually averaged shortwave CRF ~~influence~~ modified by surface albedo-cloud interactions are not yet possible, as coupled surface-atmosphere radiative transfer models capable of representing surface types like melt ponds are required to study the full seasonal cycle.~~Also for climate models with simple albedo parameterizations, the results from Fig. 5 can be interpreted as a potential bias in the shortwave F_{net} and CRF depending on the cloud optical thickness.~~

For the ACLOUD campaign, snow on sea ice was the dominant surface type (Jäkel et al., 2019), ~~which~~ transitioning from cold and fresh snow to melting snow. This explains the slightly ~~later decrease~~ delayed decline in surface albedo (Fig. 6, red scatter points) compared to SHEBA data (black)~~and represents the transition from cold and fresh snow to melting snow~~, where during this period the melt pond formation can already be identified by the rapidly decreasing surface albedo (Perovich et al., 2002). In exactly this period the transition from a positive (warming) to a negative (cooling) total (shortwave plus longwave) CRF was reported by Intrieri et al. (2002) using all-sky albedo values. Transferred to the results from Fig. 5 already without melt ponds a stronger cooling effect of ~~the~~ clouds should be expected ~~during ACLOUD.~~ by applying α_{cf}, which could also modify the onset of the total cooling effect of clouds during the ACLOUD campaign.

5 ~~Cloud radiative forcing during ACLOUDThe problems of calculating the~~ Refining the derivation of shortwave CRF~~,~~

To fulfill the requirements of the shortwave CRF definition given in Eq. 9 and thus also to take into account the processes discussed in the previous section 4, the need for a continuous estimate of the cloud-free albedo (α_{cf}) from observations under cloudy conditions becomes obvious. In addition, the application to the airborne observation during ACLOUD with the heterogeneous surface albedo environment in the MIZ requires the estimate of a representative downward shortwave irradiance ($F^{\downarrow}_{\mathrm{sw,cf}}\big|_{\alpha_{\mathrm{ar}}}$). In the following sections both aspects are discussed and the application to ACLOUD observations is demonstrated.

5.1 Considering surface albedo heterogeneities and horizontal photon transport

The observed variability of the surface albedo in the MIZ can directly be related to the variability of the observed sea ice fraction I_{f} shown in Fig. 1. Both will influence the observed field of downward shortwave irradiance, as discussed in ~~sections 3.3, 5.1 and ?? are considered in the data processing of the ACLOUD measurements. Therefore, the closest available atmospheric profile is applied in the~~ section 2.2. For the observations carried out on 23 May 2017, the measured broadband surface albedo along the flight track is shown in Fig. 7a. The low-level section started in the MIZ over large ice floes and small leads with

optically thin clouds and ended over the open ocean in the vicinity of the ice edge with occasionally scattered sea ice floe fields and optically thick clouds. Thus, leads and open water areas with the size of a few tens of meters up to a few kilometers caused a highly variable local surface albedo.

In Fig. 7b the simulated $F^{\downarrow}_{\mathrm{sw,cf}}$ using the surface albedo observed at 20 Hz illustrates the problems related to strong albedo fluctuations. The simulated $F^{\downarrow}_{\mathrm{sw,cf}}$ changes on small horizontal scales by up to 35 $\mathrm{W\,m^{-2}}$ (SZA average: 59.2°). However, due to horizontal photon transport from surrounding ice fields, in reality the changes in $F^{\downarrow}_{\mathrm{sw,cf}}$ are less pronounced. The quantitative impact of multiple scattering on $F^{\downarrow}_{\mathrm{sw,cf}}$ obtained from radiative transfer simulations ~~as well as the areal-averaged surface albedo, required for~~ is indicated by the gray shaded area in Fig. 7b with a maximum contribution of almost 40 $\mathrm{W\,m^{-2}}$ (relative to open ocean). Therefore, the downward irradiance for the cloud-free conditions, required for Eq. 9, needs to be simulated with an appropriate areal-averaged albedo representing the multiple scattering contribution from the surrounding albedo fields.

To estimate a required filter shape and width to obtain an areal-averaged albedo, 3D radiative transfer simulations of a typical scenario are performed (not shown here), where leads of different sizes are embedded in homogeneous sea ice similar to the study from Podgorny et al. (2018). The simulated irradiance of the 3D model output in the vicinity of the leads is reproduced by 1D simulations by applying the filter embedded in Fig. 7b to the ~~simulations~~ 3D modelled albedo (theoretically observed) and by using the thereby obtained areal-averaged albedo for the 1D model simulations to continuously estimate the $F^{\downarrow}_{\mathrm{sw,cf}}\big|_{\alpha_{\mathrm{ar}}}$. The appropriate weighting of near-field and far-field albedo is applied by kernel k defined by a Laplace-distribution:

$$k(x,\mu,\gamma) = \frac{1}{2\gamma}\left(-\frac{|x-\mu|}{\gamma}\right), \tag{10}$$

with γ of ~~$F^{\downarrow}_{\mathrm{sw,cf}}$, are calculated for the low-level flights. The final step is to continuously retrieve the local surface albedo under cloud-free atmospheric conditionsfrom the observed cloudy-sky albedo,~~ 5 km, the median μ and a scale x of 30 km. This rather large filter width indicates that small leads below 1 km embedded in homogeneous sea ice show a minor impact on $F^{\downarrow}_{\mathrm{sw}}$ in ~~order to obtain a more realistic~~ cloud-free conditions.

The resulting areal-averaged albedo is shown in Fig. 7a, together with the simulated $F^{\downarrow}_{\mathrm{sw,cf}}\big|_{\alpha_{\mathrm{ar}}}$ (Fig. 7b), which follows the large-scale trends of surface albedo, but mitigates small-scale fluctuations. The consequences for the local shortwave CRF estimate resulting from the neglect of these 3D effects are shown in Fig. 7c as deviation between $F^{\downarrow}_{\mathrm{sw,cf}}\big|_{\alpha_{\mathrm{ar}}}$ and $F^{\downarrow}_{\mathrm{sw,cf}}\big|_{\alpha}$. On average, the effect is of minor importance for the flight section in Fig. 7 (average -1.9 $\mathrm{W\,m^{-2}}$), because under- and overestimation of shortwave CRF cancel in this specific example, similar to results from Benner et al. (2001). On a local scale, however, it should be highlighted that due to horizontal photon transport the $F^{\downarrow}_{\mathrm{sw,cf}}\big|_{\alpha_{\mathrm{ar}}}$ is up to 28 $\mathrm{W\,m^{-2}}$ larger above leads compared to the $F^{\downarrow}_{\mathrm{sw,cf}}\big|_{\alpha}$. The difference in the derived CRF reaches values between -25 $\mathrm{W\,m^{-2}}$ over open water embedded in homogeneous sea ice, where the $F^{\downarrow}_{\mathrm{sw,cf}}$ is underestimated by applying the local albedo, and +6 $\mathrm{W\,m^{-2}}$ above scattered ice floe fields in the ocean with an overestimation of $F^{\downarrow}_{\mathrm{sw,cf}}$. Hence, the uncertainties and artificial fluctuations in CRF are limited by applying the areal-averaged albedo in the $F^{\downarrow}_{\mathrm{sw,cf}}$ simulations. This enables a more reliable estimate of the CRF ~~,~~ in the heterogeneous MIZ and over the specific surface types, taking into account that the complexity of surface albedo fields in the MIZ can only be insufficiently represented by this simplified approach to estimate the areal-averaged albedo.

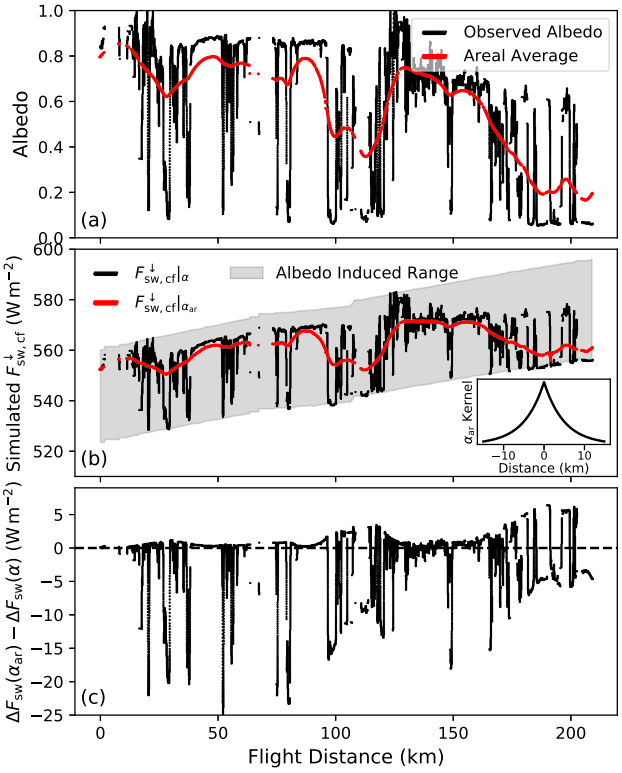

Figure 7. Time series (covered distance) of measured broadband surface albedo (black) (a) and simulated $F^{\downarrow}_{sw,cf}$ (b) along the low-level flight track during 23 May 2017. The red line in (a) shows the areal-averaged albedo using the kernel embedded in (b). (b) The gray area illustrates the potential variability of $F^{\downarrow}_{sw,cf}$ due to surface albedo changes. The black and red scatter shows the $F^{\downarrow}_{sw,cf}|_{\alpha}$ and $F^{\downarrow}_{sw,cf}|_{\alpha_{ar}}$ respectively. (c) Difference in shortwave CRF estimate between $\Delta F_{sw}(\alpha_{ar})$ and $\Delta F_{sw}(\alpha)$.

5.2 ~~Retrieving the~~ Retrieval of cloud-free albedo from cloudy-sky observations~~To obtain an~~

To obtain a continuous estimate of the cloud-free albedo (α_{cf}) during cloudy conditions as required for Eq. 9, the broadband albedo parameterization developed by Gardner and Sharp (2010) for snow and ice surfaces is applied. Gardner and Sharp (2010) considered the dependence of broadband albedo with respect to SZA, SSA, concentration of ~~absorbing carbon ,~~ light-absorbing carbon as well as the cloud optical thickness. The parameterization is valid for homogeneous snow and ice including a cloud optical thickness below 30 (LWP of 133 g m^{-2} with r_{eff} ~~=~~ of 8 µm). During ACLOUD, the observed albedo ranged between 0.9 for homogeneous sea ice covered with cold snow and values below 0.6 during the later stage of the campaign with the onset of melting (Wendisch et al., 2019; Jäkel et al., 2019). To include these data in the analysis and cover this ~~albedo range only as a function of~~ range of albedo values besides the other parameters only as function of the unknown snow grain size (SSA), an impurity load of absorbing carbon of 0.1 ppmw is chosen, which causes a similar spectral behaviour of the albedo as changes in snow thickness ~~. As shown by Jäkel et al. (2019) ,~~ (Gardner and Sharp, 2010). Although Jäkel et al. (2019) showed

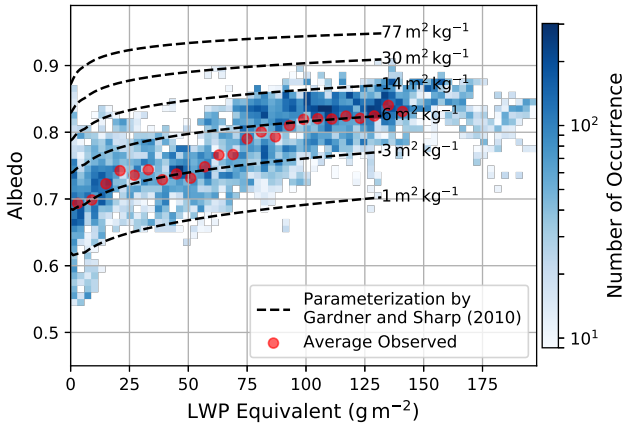

Figure 8. Relation between broadband albedo and retrieved LWP equivalent observed on 14 June 2017 ACLOUD flight over homogeneous sea ice ($I_f > 98\,\%$). The broadband albedo parameterization by Gardner and Sharp (2010) is shown for different SSA and the average SZA by the dashed lines (impurity load of 0.1 ppmw). Averaged observations (6 $\mathrm{g\,m^{-2}}$ bins) are shown in red scattered points.

that snow overlaying sea ice was the predominant surface type ~~over~~ for closed sea ice ~~during ACLOUD. Nevertheless~~conditions during ACLOUD, the potential variability in the spectral surface albedo with respect to absorption in the ~~short wavelength ranges~~ shortwave wavelength range caused by snow thickness or/and impurity fluctuations during the campaign is only roughly covered by this ~~approach~~ assumption and needs to be considered in the interpretation of the obtained cloud-free albedo values.

The parameterization is used to generate lookup tables ~~as a function of observed~~ to derive the cloud-free albedo depending on the unobserved SSA and the required variables of cloudy-sky albedo, LWP and local SZA. Isolines of SSA are used to extrapolate the cloud-free albedo (LWP = 0 $\mathrm{g\,m^{-2}}$). To apply the albedo parameterization by Gardner and Sharp (2010) the cloud optical thickness or LWP is required. As the cloud properties change on small horizontal scales, a retrieval of LWP based on the airborne measurements of cloud transmissivity was used, which is described in the ~~appendix A.~~

5.2.1 ~~Application to the observations~~

~~The~~ Appendix A.

The retrieval of LWP allows an investigation of the dependence of the surface albedo on the cloud ~~LWP~~ optical thickness, which is shown in Fig. 8 as ~~measured~~ an example for measurements over homogeneous sea ice (selected $I_f > 98\,\%$) on 14 June 2017. In addition, the albedo parameterization by Gardner and Sharp (2010) ~~for~~ is displayed for different values of SSA (isolines) and of the averaged SZA (63.7°)~~and different values of SSA is shown~~. During 1.7 hours of low-level flights below clouds, a large area was mapped (80.7-81.8° N, 9.8-12.7° E) and a strong variability in cloud optical thickness including occasional openings with direct illumination of the surface and optical thick multilayer clouds was covered. The surface temperatures were close to zero, indicating the beginning melting season (Jäkel et al., 2019). The observed albedo values averaged for 6 $\mathrm{g\,m^{-2}}$ bins (dashed red in Fig. 8) change from 0.7 for low values of LWP to albedo values above 0.8 for a LWP

~~Relation between broadband albedo and retrieved LWP equivalent observed on 14 June 2017 ACLOUD flight over homogeneous sea ice ($I_r > 98\,\%$). The broadband albedo parameterization by Gardner and Sharp (2010) is shown for different SSA and the average SZA by the dashed lines (impurity load of 0.1). Averaged observations (6 bins) are shown in red scatter.~~

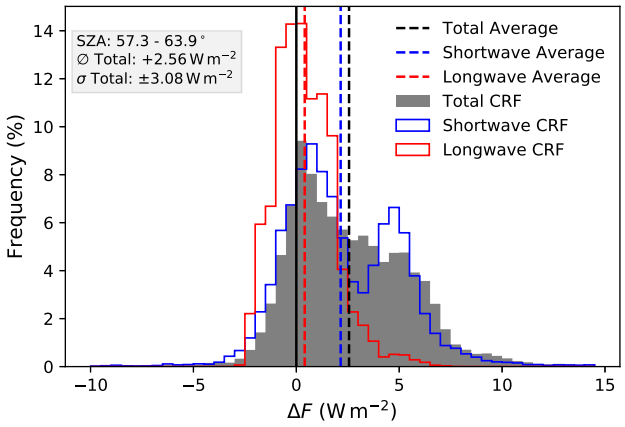

Figure 9. Histogram of shortwave, longwave and total ΔF derived during the cloud-free ACLOUD flight on 25 June 2017. Statistics are given in the gray box (mean $\varnothing$, standard deviation σ).

larger than $100\,\mathrm{g\,m^{-2}}$. While the overall trend of increasing albedo with increasing LWP is represented, the slope follows the parameterization for a SSA between $3\,\mathrm{m^2\,kg^{-1}}$ for lower LWP values and $6\,\mathrm{m^2\,kg^{-1}}$ for higher LWP. This might be related to different observed cloud and surface areas as the distribution includes data from both aircraft.

Extrapolating the observations (pair of variates) of LWP equivalent and surface albedo along isolines of SSA to a LWP of zero gives an estimate of the cloud-free surface albedo. For the example given here in Fig. 8, for a α_{all} of 0.82 and LWP of $100\,\mathrm{g\,m^{-2}}$ a cloud-free albedo of 0.74 would be estimated, and thus, 0.06 lower than the observed one in overcast conditions. For LWP values exceeding the limitation of the parameterization the maximum valid LWP was applied. Rarely occurring surface albedo values above/below the range of the parameterization from Gardner and Sharp (2010) have been filtered out. Thus, by combining temporal and spatial appropriate lookup tables (local SZA) and the observations of LWP and broadband surface albedo, a continuous estimate of α_{cf} is provided, which is suitable for the derivation of the instantaneous CRF that takes the surface albedo-cloud interaction in to account (Eq. 9).

5.3 Uncertainties

~~A comparison of measured (all-sky) α_{all} and extrapolated cloud-free albedo α_{cf} is shown in Fig. 10a . The frequency distributions are calculated for all~~ During ACLOUD, a flight in cloud-free conditions on 25 June 2017 provides the opportunity for a comparison between measured and simulated irradiances in order to estimate the accuracy of this dataset. The difference between observed and simulated $F^{\downarrow}_{\mathrm{cf}}$ for the low-level flights ~~during ACLOUD over homogeneous sea ice ($I_r > 98$~~of both aircraft (2.1 hours of data) is 5.7 ± 7.1 ~~%). The broad distribution of observed albedo illustrates the seasonal transition of sea ice~~

properties from a cold period end of May 2017 into the melting season in June 2017 (Wendisch et al., 2019; Jäkel et al., 2019). On average, the cloudy albedo (LWP > 1 $\mathrm{W\,m^{-2}}$ (1.1 %) in the shortwave and 0.41±1.45) was about 0.8. The estimated cloud-free albedo gives an average value of 0.74, which is approximately 6 $\mathrm{W\,m^{-2}}$ (0.2 % lower than α_{all}. The distribution of α_{cf} is slightly narrower than the measured one in cloudy conditions, because the majority of cloud-free flight sections took place close to %) in the longwave irradiance. The histograms of the end of CRF for that day are shown in Fig. 9. The mean values of the entire flight section is 2.15 $\mathrm{W\,m^{-2}}$ in the shortwave and 0.41 $\mathrm{W\,m^{-2}}$ in the longwave. The slightly positive CRF might be caused by the upper air sounding approximately 300 km in the south of the campaign with low values of surface albedo , and thus, gives a lower bound to the distribution.flight track or the aerosol conditions (aerosol optical thickness was set to zero in the simulation). In addition to the measurement uncertainties of the used broadband radiometer (<3 %, Ehrlich et al., 2019b), the radiative transfer modeling can induce a bias (<2 %) in the shortwave wavelength ranges (Randles et al., 2013). Due to the absence of cloud-free conditions during other low-level flights of the ACLOUD campaign this comparison can be considered as a rough estimate of potential uncertainties during the whole ACLOUD campaign.

A special aspect of this dataset concerns the measurement strategy itself, whereby the irradiances are observed in the aircraft flight altitude (during low-level sections in average 80 m) and in various atmospheric thermodynamic profiles. Radiative transfer simulations of all available profiles during the campaign indicate that the derived total CRF in flight altitude may have an offset less than ±2 $\mathrm{W\,m^{-2}}$ compared to surface-related/surface-based observation, depending on the prevailing thermodynamic profiles. Details are given in the supplement provided to this study.

In this study, the retrieval of α_{cf} is applied only above homogeneous sea ice, conditions frequently observed during ACLOUD. In the MIZ, though, the heterogeneous sea ice and the correspondingly reduced surface albedo prevents an application of the original parametrization by Gardner and Sharp (2010). In the future, however, this might become possible by making use of the cosine weighted sea ice fraction I_{f} and its linear relation to the albedo, whereby changes in surface albedo caused by the surface albedo-cloud interaction can be scaled to the prevailing I_{f} and ocean albedo by assuming diffuse radiative transfer (Lambertian albedo) (not shown in this study).

The uncertainties in the estimate retrieval of α_{cf} and the shortwave $F_{\mathrm{net,cf}}$ depend mainly on the observed α_{all}, as was investigated by applying synthetic albedo and LWP distributions to the lookup tables. Due to the non-linear increase of α_{all} with LWP, the potential error induced by uncertainties in the retrieved LWP is larger for lower LWP . Additionally, the effect and depends on the prevailing surface types. The overall uncertainty in the cloud-free shortwave net irradiances above a homogeneous high surface albedo using the retrieved α_{cf} can be expected to range should be below 20 % above homogeneous high surface albedos, decreasing and decrease with decreasing surface albedo. Fig. 10a shows only measurements conducted

6 Impact of surface albedo-cloud interaction on the CRF during ACLOUD

With the application of the methods described in section 5, the CRF during the ACLOUD campaign can be analysed with respect to the surface albedo-cloud interaction. The observed impact of clouds on the surface albedo was illustrated in Fig. 8 for one flight. A comparison of measured (all-sky) α_{all} and retrieved cloud-free albedo α_{cf} calculated for all low-level

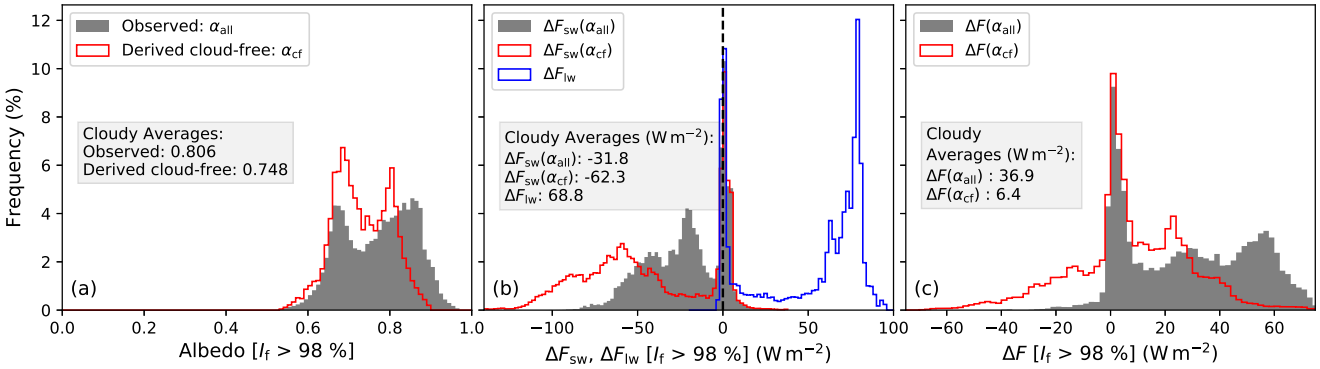

Figure 10. (a) Frequency distribution of the observed (α_{all}, gray) and cloud-free estimated (α_{cf}, red) surface albedo for all ACLOUD measurements obtained over homogeneous sea ice ($I_f > 98\,\%$). (b) Terrestrial (blue) and shortwave CRF using the observed albedo ($\Delta F_{sw}(\alpha_{all})$, gray) and the shortwave CRF applying the estimated cloud-free albedo ($\Delta F_{sw}(\alpha_{cf})$, red). (c) The total (shortwave + longwave) CRF calculated with both albedo ~~estimates are~~ parameters is shown in panel (c). Average values for cloudy conditions (LWP > 1 g m^{-2}) are given in the embedded text boxes of each panel.

flights during ACLOUD over homogeneous sea ice ~~, which was frequently observed during ACLOUD. In the MIZ, though, the heterogeneous sea ice and the corresponding reduced surface albedo prevents an application of the original parametrization by Gardner and Sharp (2010). However, making use of the cosine weighted sea ice fraction I_f and its linear relation to the albedo, changes due to the surface albedo-cloud interaction can be scaled to the prevailing I_f by assuming diffuse radiative transfer (Lambertian albedo) (not shown in this study).~~

6.1 ~~Correction of CRF~~

($I_f > 98\,\%$) is shown as frequency distributions in Fig. 10a. The broad distribution of observed albedo illustrates the seasonal transition of sea ice properties from a cold period end of May 2017 into the melting season in June 2017 (Wendisch et al., 2019; Jäkel et al., 2
On average, the α_{all} observed during cloudy conditions (LWP > 1 g m^{-2}) was about 0.8. The estimated cloud-free albedo for the same conditions gives an average value of 0.74, which is approximately 6 % lower than α_{all}. The distribution of α_{cf} is slightly narrower than the measured one in all-sky conditions, because the majority of cloud-free flight sections took place near to the end of the campaign with low values of surface albedo, and thus gives a lower bound to the distribution.

To illustrate the ~~effect of~~ effects of the surface albedo-cloud ~~interactions on the calculation of the CRF~~ interaction during the ACLOUD campaign, the CRF is computed using both the measured cloudy albedo (α_{all}) and the estimated cloud-free albedo (α_{cf}). Fig. 10b shows the frequency distribution of the shortwave CRF for both solutions, observed over homogeneous sea ice ($I_f > 98\,\%$). The CRF based on the observed albedo ($\Delta F_{sw}(\alpha_{all})$, gray bars) shows a bimodal distribution. The mode around 0 W m^{-2} represents cloud-free ~~situations~~ conditions and heterogeneous optically thin clouds, where 3D effects ~~induced~~ induce occasionally positive shortwave CRF values as reported in Wendisch et al. (2019). The broader mode between -60 W m^{-2} and

-20 $\mathrm{W\,m^{-2}}$ characterizes ~~the cloudy mode as a function of the prevailing surface albedo and LWP.~~cloudy conditions shaped by the prevailing LWP, SZA and surface albedo.

Applying the estimated cloud-free albedo ($\Delta F_{\mathrm{sw}}(\alpha_{\mathrm{cf}})$, red histogram in Fig. 10a), shifts the cloudy mode in the shortwave CRF in Fig. 10b ~~of the cloudy mode~~ to more negative values, indicating a stronger cooling effect~~. The non-linearity in the functional dependence of surface albedo and LWP spreads the frequency distribution of corrected CRF, while the mode for cloud-free conditions is not affected. In total~~, which was already implied by the radiative transfer simulations in section 4. In total, the shortwave CRF using the observed albedo values α_{all} shows on average a weak cooling effect of -32 $\mathrm{W\,m^{-2}}$ ~~using the observed albedo values~~ under cloudy conditions (LWP > 1 $\mathrm{g\,m^{-2}}$). Applying the surface albedo for cloud-free conditions almost doubles the shortwave cooling effect to -62 $\mathrm{W\,m^{-2}}$. The non-linearity in the functional dependence of surface albedo and LWP (Fig. 4 and 8) spreads the frequency distribution of $\Delta F_{\mathrm{sw}}(\alpha_{\mathrm{cf}})$ (interquartile range 36 $\mathrm{W\,m^{-2}}$ instead of 26 $\mathrm{W\,m^{-2}}$ for $\Delta F_{\mathrm{sw}}(\alpha_{\mathrm{all}})$), while the mode for cloud-free conditions is not affected. These values hold for the ACLOUD observations with an average LWP ~~during cloudy conditions over sea ice~~ of 58 $\mathrm{g\,m^{-2}}$ and a SZA of 61° ~~. In combination with the distribution of~~ during cloudy conditions over sea ice.

Under the same conditions the longwave CRF distribution (blue histogram in Fig. 10b) ~~, which~~ shows an even more distinct cloudy mode with a peak in the frequency distribution around the 78 $\mathrm{W\,m^{-2}}$ bin. During cloudy conditions (LWP > 1 $\mathrm{g\,m^{-2}}$) ΔF_{lw} averages to 69 $\mathrm{W\,m^{-2}}$ ~~in cloudy conditions, the~~ indicating a strong warming effect during this late spring early summer conditions.

The impact of surface albedo-cloud interaction becomes evident in the distribution of total (shortwave plus longwave) CRF ~~estimate~~ (Fig. 10c)~~shifts~~ , which shifts for cloudy conditions from a significant total warming effect of 37 $\mathrm{W\,m^{-2}}$ ($\Delta F(\alpha_{\mathrm{all}})$) over sea ice to an in average almost neutral effect (6 $\mathrm{W\,m^{-2}}$) by applying α_{cf}. Also the distribution of the ~~corrected CRF indicates that during the end of the campaign already the~~ $\Delta F(\alpha_{\mathrm{cf}})$ indicates that already when the α_{cf} dropped approximately below 0.75 (mid of June), the cooling effect was dominant~~(uncorrected mainly positive)~~ , meanwhile the $\Delta F_{\mathrm{sw}}(\alpha_{\mathrm{all}})$) was positive throughout the campaign. Considering that the predominant surface type of the campaign was still sea ice covered by snow, the transition from ~~warming to~~ a warming to a cooling effect of clouds could already start early in the season, even before the formation of melt ponds and the rapid ~~drop~~ decline in surface albedo (Fig. 6), which underlines the potential impact of surface albedo-cloud interactions.

7 Summary and conclusions

To estimate the warming or cooling effect of clouds on the ~~surface REB in the Arctic~~ Arctic surface from observations or models, a precise characterization of the cloud-free state is required~~. Especially in the~~ , which serves as a reference. Although the radiative cloud-free state constructed from cloudy observations remains an apparently theoretical construct with freedom of interpretation and definition, there are several relevant aspects for the characterization of the CRF in the Arctic, which are listed in the points below.

- In the transition region between open ocean and closed sea ice (the MIZ), the thermodynamic state of the atmosphere changes on horizontal scales of a few kilometers (Lampert et al., 2012), which influences the ~~simulated~~ cloud-free reference state and the resulting simulated radiative field. ~~Also, to~~ To obtain reliable estimates of CRF along meridional air mass transports into and out of the Arctic, such as warm air intrusions or cold air outbreaks (Tjernström et al., 2015; Pithan et al., 2018; Tjernström et al., 2019), a high temporal and spatial resolution of thermodynamic profile measurements along the trajectory ~~are required.~~ close to the MIZ is required. In this paper we could prove the importance of this effect using observations collected during a warm air advection case in early summer showing relatively weak related thermodynamic changes, but a considerable impact on the estimate of CRF.

- Variability in sea ice concentration is closely linked with fluctuations in surface albedo. The derivation of downward shortwave irradiances under cloud-free conditions in heterogeneous surface albedo conditions requires an estimate of the effective areal average surface albedo, determining the multiple scattering on large spatial scales ~~. For airborne observations,~~ (e.g., Kreuter et al., 2014). For the airborne observations collected during ACLOUD, we illustrate that moving average filters with shapes appropriate ~~of reproducing~~ to reproduce 3D radiative transfer need to be applied to obtain values of shortwave CRF ~~adapted to the environment.~~ considering horizontal surface albedo inhomogeneities appropriately.

- The transition between cloudy and cloud-free atmospheric states is accompanied by changes in the radiative transfer, affecting the surface albedo, and the CRF. In the available CRF studies in the Arctic, either observations during cloud-free periods have been used to extrapolate the expected cloud-free surface albedo during cloudy periods, or ~~simply~~ the surface albedo observed in cloudy conditions have been used. ~~As~~ However, as the snow and ice albedo depends on parameters like snow grain size, prevailing SZA, and cloud optical thickness, the available approaches only insufficiently represent the cloud-free albedo in the cloudy Arctic.

- Changes in shortwave surface albedo with increasing cloud optical thickness are considerable and directly impact the shortwave net irradiances, and thus, the estimate of shortwave CRF. Combining spectral snow surface albedo models with atmospheric radiative transfer simulations enables ~~to quantify the impact of two processes related to~~ us to characterize the two processes involved in spectral surface albedo-cloud interactions and to assess the importance of these effects on shortwave CRF as a function of cloud LWP and SZA for three common surface types in the Arctic (fresh snow, melting snow and sea ice). The spectral weighting effect of downward irradiance appears to be dominant for snow surfaces and enhances the cooling effect of clouds at the surface. For the second process, a change from mainly direct radiation in the cloud-free state to rather diffuse radiation in the cloudy state, the sign of the modification depends on SZA, cloud optical thickness, and the melting state of sea ice. ~~The changes in shortwave surface albedo with increasing cloud optical thickness are significant and directly impact the shortwave net irradiances, and thus, the estimate of shortwave CRF.~~

- For the ACLOUD campaign, characterized by snow on sea ice in the beginning melting season, the averaged shortwave CRF estimate over homogeneous sea ice of -32 $\mathrm{W\,m^{-2}}$ (cooling) almost doubles to -62 $\mathrm{W\,m^{-2}}$, when surface

albedo-cloud interactions are taken into account ~~. The~~ by using the proposed retrieval of cloud-free albedo from cloudy observations. Due to this consideration, the campaign averaged total (shortwave plus longwave) CRF is shifted from a mainly warming effect of clouds over sea ice to an almost neutral effect, for the ACLOUD observations with relatively small SZA. ~~Hence, the observed~~

- The observed surface albedo trend during the ACLOUD campaign (Fig. 6) induces a transition ~~in~~ of the CRF from a warming to a cooling already for snow covered surface types, and thus, earlier in the season ~~as~~ than reported during SHEBA. In addition, the instantaneous longwave CRF approach might additionally induce an overestimate of the warming effect (section 2) potentially shifting the total CRF further to cooling. This indicates a possible extension of the period in which clouds cool the surface and highlights the impact of surface albedo-cloud interactions and a required reassessment of the CRF in the Arctic.

Long-term measurements, such as those performed during the SHEBA campaign or currently within the Multidisciplinary drifting Observatory for the Study of Arctic Climate (MOSAiC) expedition (www.mosaic-expedition.org), with an appropriate instrumentation and radiative transfer ~~modelling~~ modeling will be required to quantify these effects and their potential seasonal dependence by continuously estimating the cloud-free albedo in cloudy conditions. The proposed method to estimate the surface albedo in cloud-free conditions using the parameterization from Gardner and Sharp (2010) can be easily applied to common Arctic long-term observations above snow and ice surface types, especially if high quality LWP measurements are available.

Besides observations, global climate models ~~and their estimate of~~ estimate the cloud radiative feedback ~~are~~ based on the impact of clouds on the surface REB, for which the surface albedo is fundamental. For specific surface types, often fixed values of shortwave surface albedo are assigned and parameterized using surface temperature. However, these simplified parameterizations are not appropriate to accurately describe surface albedo-cloud interactions. The use of parameterizations accounting for these effects, such as that of Gardner and Sharp (2010), are necessary and highlight the need for coupled surface atmosphere models including representative surface microphysical properties. The shortwave net irradiances depend not alone on cloud transmissivity and surface albedo, moreover the interaction between both needs to be represented.

Further effort in coupled surface atmosphere radiative transfer ~~modelling~~ modeling with a representation of common surface albedo types, like the ones from melt ponds in the Arctic, are required to track the seasonal cycle of shortwave CRF. Spectral albedo observations combined with the common broadband devices will help to account for the spectral features in surface albedo and trace changes in SSA. The proposed approach of reproducing the cloud-free albedo can not adequately reflect the diversity of spectral surface albedo types and issues related to the surface albedo-cloud interaction, especially in summer.

Considering the surface albedo-cloud interaction in global climate models and upcoming long-term observations such as MOSAiC will further improve our understanding of CRF and cloud radiative feedback in the Arctic environment and its role for Arctic amplification.

Data availability. The pyranometer and pyrgeometer broadband irradiance and KT-19 nadir brightness temperature from AWI aircraft Polar 5&6 during the May to June 2017 ACLOUD campaign are published on the PANGAEA database (Stapf et al., 2019a). The retrieved quantities of CRF, LWP equivalent and cloud-free albedo are available on the PANGAEA database (Stapf et al., 2019b). Air temperature, relative humidity and pressure in situ profiles from both aircraft are used from (Hartmann et al., 2019). Polar 5 Dropsondes: (Ehrlich et al., 2019a). Calibrated fisheye camera images: (Jäkel and Ehrlich, 2019; Jäkel et al., 2019). Radiosoundings from Polarstern (Schmithüsen, 2017) and Ny-Ålesund (Maturilli, 2017a, b).

Appendix A: Transmissivity-based retrieval of LWP equivalent

The cloud transmissivity is defined by the ratio of measured $F^{\downarrow}_{\mathrm{sw,all}}$ and the simulated cloud-free $F^{\downarrow}_{\mathrm{sw,cf}}$ downward irradiance:

$$\mathcal{T} = \frac{F^{\downarrow}_{\mathrm{sw,all}}}{F^{\downarrow}_{\mathrm{sw,cf}}}. \tag{A1}$$

$\mathcal{T}$ can be converted into cloud optical thickness or LWP, however, it is important to account for the surface albedo dependences due to multiple scattering. The $\mathcal{T}$ for a cloud with the same microphysical properties over snow and ice is higher compared to over open ocean, where the majority of photons will be absorbed by the surface and are not available for new back-scattering events of the upward irradiance in the cloud towards the surface. Taking this dependence into account, the broadband $\mathcal{T}$ is used to derive the cloud optical thickness similar to the approach by Leontyeva and Stamnes (1993).

Lookup tables of $\mathcal{T}$ for a range of surface albedo between 0 and 1 and LWP between 0 and 320 $\mathrm{g\,m^{-2}}$ are simulated for the local solar zenith angle and thermodynamic profile and subsequently compared to the values derived from the observations along the flight track. In the simulations, vertically homogeneous pure liquid water clouds are assumed to limit the complexity of the simulations. ~~Therefore, in the following~~In the following, therefore, the LWP is referred to an equivalent LWP, because no ice water content is assumed. The cloud is located between 400 m and 600 m with a fixed r_{eff} of 8 µm, typical for Arctic clouds in this season and region (Mioche et al., 2017). These rather crude assumptions result in uncertainties of the simulated irradiance, which were quantified by Leontyeva and Stamnes (1993) as a function of surface albedo, SZA, r_{eff} and cloud optical thickness.

Similar to the simulations of $F^{\downarrow}_{\mathrm{sw,cf}}$ for heterogeneous surface albedo fields, an effective albedo, which influences the local scattering processes in cloudy conditions needs to be considered in the retrieval simulations of $\mathcal{T}$ (Pirazzini and Raisanen, 2008).

The diversity of potential 3D effects induced by surface and cloud heterogeneities in the MIZ omit a specific solution for the smoothing problem of the ~~areal averaged~~ areal-averaged effective albedo and can only partially be depicted by radiative transfer ~~modelling~~modeling. To make the retrieval applicable to ACLOUD measurements and reduce the uncertainties induced by horizontal photon transport, a commonly observed cloud/surface scene, with a cloud base height of 200 m and leads with different sizes, are simulated using 3D radiative transfer (not shown here). The estimated kernel k is based on a Cauchy

distribution:

$$k(x,\mu,\gamma) = \left(\pi \cdot \gamma \cdot \left[1 + \left(\frac{x-\mu}{\gamma}\right)^2\right]\right)^{-1}, \tag{A2}$$

with γ of 400 m, the median μ and a scale x of 10 km. The horizontal extent is, as expected, smaller compared to the cloud-free kernel introduced in Fig. 7b, due to the low cloud base height limiting the free photon path length. Applied to the ~~theoretical observed~~3D modelled (theoretically observed) albedo the simulated 1D irradiance adequately reproduces the results obtained from the 3D output, and thus, reduces for these cloud/surface scenes the uncertainties of the retrieved LWP considerably.

Nevertheless, multiple scattering, changes in cloud base height (Pirazzini and Raisanen, 2008) and 3D radiative effects due to inhomogeneous cloud/surface scenes, might induce large uncertainties in this retrieval. However, the observed I_f statistics indicate that the majority of ACLOUD flights were conducted over a rather homogeneous surface, where the discussed issue is ~~minor important~~of minor importance. The sensitivity of the retrieval is in general higher over open water compared to over ice, since changes in $F^{\downarrow}_{\mathrm{sw}}$ with increasing LWP are more pronounced. The relative uncertainty ~~range~~ of this retrieval for homogeneous clouds and ~~surface~~ surfaces can be expected to range between 15 % and 35 % over open ocean and sea ice~~respectively.~~, respectively.

The conversion from LWP to optical thickness (τ), as required for the parameterization by Gardner and Sharp (2010), is applied by,

$$\tau = \frac{9}{5} \cdot \frac{\mathrm{LWP}}{\varrho_\mathrm{w} \cdot r_\mathrm{eff}}, \tag{A3}$$

with the density of liquid water ϱ_w and the simulated r_eff.

Author contributions. All authors contributed to the editing of the manuscript and to the discussion of the results. JS drafted the manuscript and initialized the study. JS processed the radiation data, merged the data sets and performed the radiative transfer simulations. EJ contributed to the radiative transfer simulations and their interpretation. MW, AE and CL designed the experimental basis of this study.

Competing interests. The authors declare that they have no conflict of interest.

Acknowledgements. We gratefully acknowledge the funding by the Deutsche Forschungsgemeinschaft (DFG, German Research Foundation) – Project Number 268020496 – TRR 172, within the Transregional Collaborative Research Center "ArctiC Amplification: Climate Relevant Atmospheric and SurfaCe Processes, and Feedback Mechanisms (AC)³". The authors are grateful to AWI for providing and operating the two aircraft during the ACLOUD campaign. We thank the crews of Polar 5 and Polar 6, the technicians of the aircraft for excellent technical and logistical support. The generous funding of the flight hours for ACLOUD by AWI is greatly appreciated. Observations in Fig. 6 were made by the SHEBA Atmospheric Surface Flux Group, Ed Andreas, Chris Fairall, Peter Guest, and Ola Persson. Data provided by NCAR/EOL under the sponsorship of the National Science Foundation (https://data.eol.ucar.edu/).

References

Allan, R. P. and Ringer, M. A.: Inconsistencies between satellite estimates of longwave cloud forcing and dynamical fields from reanalyses, Geophys. Res. Lett., 30, 1491, https://doi.org/10.1029/2003GL017019, 2003.

Anderson, G., Clough, S., Kneizys, F., Chetwynd, J., and Shettle, E.: AFGL Atmospheric Constituent Profiles (0–120 km), Tech. Rep. AFGL-TR-86-0110, AFGL (OPI), Hanscom AFB, MA 01736, 1986.

Benner, T. C., Curry, J. A., and Pinto, J. O.: Radiative transfer in the summertime Arctic, J. Geophys. Res., 106, 15.173–15.183, 2001.

Cohen, J., Screen, J. A., Furtado, J. C., Barlow, M., Whittleston, D., Coumou, D., Francis, J., Dethloff, K., Entekhabi, D., Overland, J., and Jones, J.: Recent Arctic amplification and extreme mid-latitude weather, Nat. Geosci., 7, 627–637, https://doi.org/10.1038/NGEO2234, 2014.

Cox, C. J., Walden, V. P., Rowe, P. M., and Shupe, M. D.: Humidity trends imply increased sensitivity to clouds in a warming Arctic, Nat. Commun., 6, 10 117, https://doi.org/10.1038/ncomms10117, 2015.

Cox, C. J., Uttal, T., Long, C. N., Shupe, M. D., Stone, R. S., and Starkweather, S.: The Role of Springtime Arctic Clouds in Determining Autumn Sea Ice Extent, J. Climate, 29, 6581–6596, https://doi.org/10.1175/JCLI-D-16-0136.1, 2016.

Dong, X. Q., Xi, B. K., and Minnis, P.: A climatology of midlatitude continental clouds from the ARM SGP central facility. Part II: Cloud fraction and surface radiative forcing, J. Climate, 19, 1765–1783, 2006.

Dong, X. Q., Xi, B. K., Crosby, K., Long, C. N., Stone, R. S., and Shupe, M. D.: A 10 year climatology of Arctic cloud fraction and radiative forcing at Barrow, Alaska RID F-8754-2011, J. Geophys. Res., 115, D17 212, https://doi.org/10.1029/2009JD013489, 2010.

Ehrlich, A., Stapf, J., Lüpkes, C., Mech, M., Crewell, S., and Wendisch, M.: Meteorological measurements by dropsondes released from POLAR 5 during ACLOUD 2017, PANGAEA, https://doi.org/10.1594/PANGAEA.900204, 2019a.

Ehrlich, A., Wendisch, M., Lüpkes, C., Buschmann, M., Bozem, H., Chechin, D., Clemen, H.-C., Dupuy, R., Eppers, O., Hartmann, J., Herber, A., Jäkel, E., Järvinen, E., Jourdan, O., Kästner, U., Kliesch, L.-L., Köllner, F., Mech, M., Mertes, S., Neuber, R., Ruiz-Donoso, E., Schnaiter, M., Schneider, J., Stapf, J., and Zanatta, M.: A comprehensive in situ and remote sensing data set from the Arctic CLoud Observations Using airborne measurements during polar Day (ACLOUD) campaign., Earth Syst. Sci. Data Discuss., https://doi.org/10.5194/essd-2019-96, in review, 2019b.

Emde, C., Buras-Schnell, R., Kylling, A., Mayer, B., Gasteiger, J., Hamann, U., Kylling, J., Richter, B., Pause, C., Dowling, T., and Bugliaro, L.: The libRadtran software package for radiative transfer calculations (version 2.0.1), Geosci. Model Dev., 9, 1647–1672, https://doi.org/10.5194/gmd-9-1647-2016, 2016.

Gardner, A. S. and Sharp, M. J.: A review of snow and ice albedo and the development of a new physically based broadband albedo parameterization, J. Geophys. Res., 115, F01 009, https://doi.org/10.1029/2009JF001444, 2010.

Gasteiger, J., Emde, C., Mayer, B., Buras, R., Buehler, S. A., and Lemke, O.: Representative wavelengths absorption parameterization applied to satellite channels and spectral bands, J. Quant. Spectrosc. Ra., 148, 99–115, https://doi.org/10.1016/j.jqsrt.2014.06.024, 2014.

Gillett, N. P., Stone, D. A., Stott, P. A., Nozawa, T., Karpechko, A. Y., Hegerl, G. C., Wehner, M. F., and Jones, P. D.: Attribution of polar warming to human influence, Nat. Geosci., 1, 750–754, https://doi.org/10.1038/ngeo338, 2008.

Goosse, H., Kay, J. E., Armour, K. C., Bodas-Salcedo, A., Chepfer, H., Docquier, D., Jonko, A., Kushner, P. J., Lecomte, O., Massonnet, F., Park, H. S., Pithan, F., Svensson, G., and Vancoppenolle, M.: Quantifying climate feedbacks in polar regions, Nat. Commun., 9, 1919, https://doi.org/10.1038/s41467-018-04173-0, 2018.

Grenfell, T. C. and Perovich, D. K.: Incident spectral irradiance in the Arctic Basin during the summer and fall, J. Geophys. Res., 113, D12 117, https://doi.org/10.1029/2007JD009418, 2008.

Hartmann, J., Lüpkes, C., and Chechin, D.: High resolution aircraft measurements of wind and temperature during the ACLOUD campaign in 2017, PANGAEA, https://doi.pangaea.de/10.1594/PANGAEA.900880, 2019.

Hori, M., Aoki, T., Tanikawa, T., Motoyoshi, H., Hachikubo, A., Sugiura, K., Yasunari, T. J., Eide, H., Storvold, R., Nakajima, Y., and Takahashi, F.: In-situ measured spectral directional emissivity of snow and ice in the 8-14 mu m atmospheric window, Remote Sens. Environ., 100, 486–502, https://doi.org/10.1016/j.rse.2005.11.001, 2006.

Intrieri, J. M., Fairall, C. W., Shupe, M. D., Persson, P. O. G., Andreas, E. L., Guest, P. S., and Moritz, R. E.: An annual cycle of Arctic surface cloud forcing at SHEBA, J. Geophys. Res., 107, 8039, 2002.

Iwabuchi, H.: Efficient Monte Carlo methods for radiative transfer modeling, J. Atmos. Sci., 63, 2324–2339, 2006.

Iwabuchi, H. and Kobayashi, H.: Modeling of radiative transfer in cloudy atmospheres and plant canopies using Monte Carlo methods, Tech. Rep., 8, 199 pp., 2008.

Jäkel, E. and Ehrlich, A.: Radiance fields of clouds and the Arctic surface measured by a digital camera during ACLOUD 2017, PANGAEA, https://doi.pangaea.de/10.1594/PANGAEA.901024, 2019.

Jäkel, E., Stapf, J., Wendisch, M., Nicolaus, M., Dorn, W., and Rinke, A.: Validation of the sea ice surface albedo scheme of the regional climate model HIRHAM-NAOSIM using aircraft measurements during the ACLOUD/PASCAL campaigns, Cryosphere, 13, 1695–1708, https://doi.org/10.5194/tc-13-1695-2019, 2019.

Jeffries, M. O., Overland, J. E., and Perovich, D. K.: The Arctic shifts to a new normal, Phys. Today, 66, 35–40, 2013.

Kato, S., Ackerman, T., Mather, J., and Clothiaux, E.: The k-distribution method and correlated-k approximation for a shortwave radiative transfer model, J. Quant. Spectrosc. Ra., 62, 109–121, 1999.

Knudsen, E. M., Heinold, B., Dahlke, S., Bozem, H., Crewell, S., Gorodetskaya, I. V., Heygster, G., Kunkel, D., Maturilli, M., Mech, M., Viceto, C., Rinke, A., Schmithüsen, H., Ehrlich, A., Macke, A., Lüpkes, C., and Wendisch, M.: Meteorological conditions during the ACLOUD/PASCAL field campaign near Svalbard in early summer 2017, Atmos. Chem. Phys., 18, 17 995–18 022, https://doi.org/10.5194/acp-18-17995-2018, 2018.

Kreuter, A., Buras, R., Mayer, B., Webb, A., Kift, R., Bais, A., Kouremeti, N., and Blumthaler, M.: Solar irradiance in the heterogeneous albedo environment of the Arctic coast: measurements and a 3-D model study, Atmos. Chem. Phys., 14, 5989–6002, https://doi.org/10.5194/acp-14-5989-2014, 2014.

Lampert, A., Maturilli, M., Ritter, C., Hoffmann, A., Stock, M., Herber, A., Birnbaum, G., Neuber, R., Dethloff, K., Orgis, T., Stone, R., Brauner, R., Kassbohrer, J., Haas, C., Makshtas, A., Sokolov, V., and Liu, P.: The spring-time boundary layer in the central Arctic observed during PAMARCMiP 2009, Atmosphere-Basel, 3, 320–351, https://doi.org/10.3390/atmos3030320, 2012.

Leontyeva, E. and Stamnes, K.: Estimation of cloud optical thickness from ground-based measurements of incoming solar radiation in the Arctic, J. Climate, 7, 566–578, 1993.

Libois, Q., Picard, G., France, J. L., Arnaud, L., Dumont, M., Carmagnola, C. M., and King, M. D.: Influence of grain shape on light penetration in snow, Cryosphere, 7, 1803–1818, https://doi.org/10.5194/tc-7-1803-2013, 2013.

Long, C. and Ackerman, T.: Identification of clear skies from broadband pyranometer measurements and calculation of downwelling shortwave cloud effects, J. Geophys. Res., 105, 15 609–15 626, 2000.

Long, C. N.: On the estimation of clear-sky upwelling SW and LW, Fifteenth ARM Science Team Meeting Proceedings, Daytona Beach, Florida, March 14–18, 2005.

Long, C. N. and Turner, D. D.: A method for continuous estimation of clear-sky downwelling longwave radiative flux developed using ARM surface measurements, J. Geophys. Res., 113, D18 206, https://doi.org/10.1029/2008JD009936, 2008.

Maturilli, M.: High resolution radiosonde measurements from station Ny-Ålesund (2017-05), PANGAEA, https://doi.org/10.1594/PANGAEA.879820, 2017a.

Maturilli, M.: High resolution radiosonde measurements from station Ny-Ålesund (2017-06), PANGAEA, https://doi.org/10.1594/PANGAEA.879822, 2017b.

Miller, N. B., Shupe, M. D., Cox, C. J., Walden, V. P., Turner, D. D., and Steffen, K.: Cloud Radiative Forcing at Summit, Greenland, J. Climate, 28, 6267–6280, https://doi.org/10.1175/JCLI-D-15-0076.1, 2015.

Miller, N. B., Shupe, M. D., Lenaerts, J. T. M., Kay, J. E., de Boer, G., and Bennartz, R.: Process-Based Model Evaluation Using Surface Energy Budget Observations in Central Greenland, J. Geophys. Res., 123, 4777–4796, https://doi.org/10.1029/2017JD027377, 2018.

Mioche, G., Jourdan, O., Delanoe, J., Gourbeyre, C., Febvre, G., Dupuy, R., Monier, M., Szczap, F., Schwarzenboeck, A., and Gayet, J. F.: Vertical distribution of microphysical properties of Arctic springtime low-level mixed-phase clouds over the Greenland and Norwegian seas, Atmos. Chem. Phys., 17, 12 845–12 869, https://doi.org/10.5194/acp-17-12845-2017, 2017.

Overland, J. E., Wood, K. R., and Wang, M.: Warm Arctic–cold continents: Impacts of the newly open Arctic Sea, Polar Res., 30, 15 787, doi:10.3402/polar.v30i0.15 787, 2011.

Perovich, D. K., Grenfell, T. C., Light, B., and Hobbs, P. V.: Seasonal evolution of the albedo of multiyear Arctic sea ice, J. Geophys. Res., 107, https://doi.org/10.1029/2000JC000438, 8044, 2002.

Pirazzini, R. and Raisanen, P.: A method to account for surface albedo heterogeneity in single-column radiative transfer calculations under overcast conditions, J. Geophys. Res., 113, https://doi.org/10.1029/2008JD009815, 2008.

Pithan, F. and Mauritsen, T.: Arctic amplification dominated by temperature feedbacks in contemporary climate models, Nature, 7, 181–184, https://doi.org/10.1038/ngeo2071, 2014.

Pithan, F., Svensson, G., Caballero, R., Chechin, D., Cronin, T. W., Ekman, A. M. L., Neggers, R., Shupe, M. D., Solomon, A., Tjernstrom, M., and Wendisch, M.: Role of air-mass transformations in exchange between the Arctic and mid-latitudes, Nat. Geosci., 11, 805–812, https://doi.org/10.1038/s41561-018-0234-1, 2018.

Podgorny, I., Lubin, D., and Perovich, D. K.: Monte Carlo Study of UAV-Measurable Albedo over Arctic Sea Ice, J. Atmos. Ocean. Tech., 35, 57–66, https://doi.org/10.1175/JTECH-D-17-0066.1, 2018.

Ramanathan, V., Cess, R, D., Harrison, E. F., Minnis, P., Barkstrom, B. R., Ahmad, E., and Hartmann, D.: Cloud-radiative forcing and climate: Results from the Earth Radiation Biudget Experiment, Science, 243, 57–63, 1989.

Randles, C. A., Kinne, S., Myhre, G., Schulz, M., Stier, P., Fischer, J., Doppler, L., Highwood, E., Ryder, C., Harris, B., Huttunen, J., Ma, Y., Pinker, R. T., Mayer, B., Neubauer, D., Hitzenberger, R., Oreopoulos, L., Lee, D., Pitari, G., Di Genova, G., Quaas, J., Rose, F. G., Kato, S., Rumbold, S. T., Vardavas, I., Hatzianastassiou, N., Matsoukas, C., Yu, H., Zhang, F., Zhang, H., and Lu, P.: Intercomparison of shortwave radiative transfer schemes in global aerosol modeling: results from the AeroCom Radiative Transfer Experiment, Atmos. Chem. Phys., 13, 2347–2379, https://doi.org/10.5194/acp-13-2347-2013, 2013.

Ricchiazzi, P. and Gautier, C.: Investigation of the effect of surface heterogeneity and topography on the radiation environment of Palmer Station, Antarctica, with a hybrid 3-D radiative transfer model, J. Geophys. Res., 103, 6161–6178, 1998.

Roode, S. and Bretherton, C.: Integrated observational dataset for model validation. Version 1.0. UCAR/NCAR - Earth Observing Laboratory, https://data.eol.ucar.edu/dataset/13.818, 2007.

Schmithüsen, H.: Upper air soundings during POLARSTERN cruise PS106.1 (ARK-XXXI/1.1), PANGAEA, https://doi.org/10.1594/PANGAEA.882736, 2017.

Screens, J. A. and Simmonds, I.: The central role of diminishing sea ice in recent Arctic temperature amplification, Nature, 464, 1334–1337, 2010.

Sedlar, J., Tjernstrom, M., Mauritsen, T., Shupe, M. D., Brooks, I. M., Persson, P. O. G., Birch, C. E., Leck, C., Sirevaag, A., and Nicolaus, M.: A transitioning Arctic surface energy budget: the impacts of solar zenith angle, surface albedo and cloud radiative forcing RID F-8754-2011, Climate Dyn., 37, 1643–1660, https://doi.org/10.1007/s00382-010-0937-5, 2011.

Serreze, M. C. and Barry, R. G.: Processes and impacts of Arctic amplification: A research synthesis, Global Planet. Change, 77, 85–96,doi:10.1016/j.gloplacha.2011.03.004, 2011.

Shupe, M. D. and Intrieri, J. M.: Cloud radiative forcing of the Arctic surface: The influence of cloud properties, surface albedo, and solar zenith angle, J. Climate, 17, 616–628, 2004.

Shupe, M. D., Walden, V. P., Eloranta, E., Uttal, T., Campbell, J. R., Starkweather, S. M., and Shiobara, M.: Clouds at Arctic Atmospheric Observatories. Part I: Occurrence and Macrophysical Properties, J. Appl. Meteorol., 50, 626–644, https://doi.org/10.1175/2010JAMC2467.1, 2011.

Spreen, G., Kaleschke, L., and Heygster, G.: Sea ice remote sensing using AMSR-E 89-GHz channels, J. Geophys. Res., 113, C02S03, https://doi.org/10.1029/2005JC003384, 2008.

Stamnes, K., Tsay, S., Wiscombe, W., and Jayaweera, K.: A numerically stable algorithm for discrete-ordinate-method radiative transfer in multiple scattering and emitting layered media, Appl. Opt., 27, 2502–2509, 1988.

Stapf, J., Ehrlich, A., Jäkel, E., and Wendisch, M.: Aircraft measurements of broadband irradiance during the ACLOUD campaign in 2017, PANGAEA, https://doi.org/10.1594/PANGAEA.900442, ~~2019.~~ 2019a.

Stapf, J., Ehrlich, A., Jäkel, E., and Wendisch, M.: Cloud radiative forcing, LWP and cloud-free albedo derived from airborne broadband irradiance observations during the ACLOUD campaign, PANGAEA, https://doi.org/10.1594/PANGAEA.909289, 2019b.

Stramler, K., Del Genio, A. D., and Rossow, W. B.: Synoptically Driven Arctic Winter States, J. Climate, 24, 1747–1762, https://doi.org/10.1175/2010JCLI3817.1, 2011.

Stroeve, J. C., Serreze, M. C., Holland, M. M., Kay, J. E., Maslanik, J., and Barrett, A. P.: The Arctic's rapidly shrinking sea ice cover: A research synthesis, Climatic Change, 110, 1005–1027, doi:10.1007/s10 584–011–0101–1, 2012.

Tjernström, M. and Graversen, R. G.: The vertical structure of the lower Arctic troposphere analysed from observations and the ERA-40 reanalysis, Quart. J. Roy. Meteor. Soc., 135, 431–443, https://doi.org/10.1002/qj.380, 2009.

Tjernström, M., Shupe, M. D., Brooks, I. M., Persson, P. O. G., Prytherch, J., Salisbury, D. J., Sedlar, J., Achtert, P., Brooks, B. J., Johnston, P. E., Sotiropoulou, G., and Wolfe, D.: Warm-air advection, air mass transformation and fog causes rapid ice melt, Geophys. Res. Lett., 42, 5594–5602, https://doi.org/10.1002/2015GL064373, 2015.

Tjernström, M., Shupe, M. D., Brooks, I. M., Achtert, P., Prytherch, J., and Sedlar, J.: Arctic Summer Airmass Transformation, Surface Inversions, and the Surface Energy Budget, J. Climate, 32, 769–789, https://doi.org/10.1175/JCLI-D-18-0216.1, 2019.

Uttal, T., Curry, J. A., McPhee, M. G., Perovich, D. K., Moritz, R. E., Maslanik, J. A., Guest, P. S., Stern, H. L., Moore, J. A., Turenne, R., Heiberg, A., Serreze, M. C., Wylie, D. P., Persson, O. G., Paulson, C. A., Halle, C., Morison, J. H., Wheeler, P. A., Makshtas, A., Welch, H., Shupe, M. D., Intrieri, J. M., Stamnes, K., Lindsey, R. W., Pinkel, R., Pegau, W. S., Stanton, T. P., and Grenfeld, T. C.: Surface heat budget of the Arctic Ocean, B. Am. Meteorol. Soc., 83, 255–275, https://doi.org/10.1175/1520-0477(2002)083<0255:SHBOTA>2.3.CO;2, 2002.

Walsh, J. E. and Chapman, W. L.: Arctic cloud-radiation-temperature associations in observational data and atmospheric reanalyses, J. Climate, 11, 3030–3045, https://doi.org/10.1175/1520-0442(1998)011<3030:ACRTAI>2.0.CO;2, 1998.

Wang, W. S., Zender, C. S., and van As, D.: Temporal Characteristics of Cloud Radiative Effects on the Greenland Ice Sheet: Discoveries From Multiyear Automatic Weather Station Measurements, J. Geophys. Res., 123, 11 348–11 361, https://doi.org/10.1029/2018JD028540, 2018.

Warren, S.: Optical Properties of Snow, Rev. Geophys. Space Phys., 20, 67–89, 1982.

Weihs, P., Lenoble, J., Blumthaler, M., Martin, T., Seckmeyer, G., Philipona, R., de la Casiniere, A., Sergent, C., Gröbner, J., Cabot, T., Masserot, D., Pichler, T., Pougatch, E., Rengarajan, G., Schmucki, D., and Simic, S.: Modeling the effect of an inhomogeneous surface albedo on incident UV radiation in mountaineous terrain: determination of an effective surface albedo, Geophys. Res. Lett., 28, 3111–3114, 2001.

Wendisch, M., Pilewskie, P., Jäkel, E., Schmidt, S., Pommier, J., Howard, S., Jonsson, H. H., Guan, H., Schröder, M., and Mayer, B.: Airborne measurements of areal spectral surface albedo over different sea and land surfaces, J. Geophys. Res., 109, Art. No. D08 203, https://doi.org/doi:10.1029/2003JD004392, 2004.

Wendisch, M., Brückner, M., Burrows, J. P., Crewell, S., Dethloff, K., Ebell, K., Lüpkes, C., Macke, A., Notholt, J., Quaas, J., Rinke, A., and Tegen, I.: Understanding causes and effects of rapid warming in the Arctic, Eos, 98, https://doi.org/10.1029/2017EO064803, 2017.

Wendisch, M., Macke, A., Ehrlich, A., Lüpkes, C., Mech, M., Chechin, D., Barrientos, C., Bozem, H., Brückner, M., Clemen, H.-C., Crewell, S., Donth, T., Dupuy, R., Ebell, K., Egerer, U., Engelmann, R., Engler, C., Eppers, O., Gehrmann, M., Gong, X., Gottschalk, M., Gourbeyre, C., Griesche, H., Hartmann, J., Hartmann, M., Herber, A., Herrmann, H., Heygster, G., Hoor, P., Jafariserajehlou, S., Jäkel, E., Järvinen, E., Jourdan, O., Kästner, U., Kecorius, S., Knudsen, E. M., Köllner, F., Kretzschmar, J., Lelli, L., Leroy, D., Maturilli, M., Mei, L., Mertes, S., Mioche, G., Neuber, R., Nicolaus, M., Nomokonova, T., Notholt, J., Palm, M., van Pinxteren, M., Quaas, J., Richter, P., Ruiz-Donoso, E., Schäfer, M., Schmieder, K., Schnaiter, M., Schneider, J., Schwarzenböck, A., Seifert, P., Shupe, M. D., Siebert, H., Spreen, G., Stapf, J., Stratmann, F., Vogl, T., Welti, A., Wex, H., Wiedensohler, A., Zanatta, M., and Zeppenfeld, S.: The Arctic cloud puzzle: using ACLOUD/PASCAL multi-platform observations to unravel the role of clouds and aerosol particles in Arctic amplification, B. Am. Meteorol. Soc., 100 (5), 841–871, https://doi.org/10.1175/BAMS-D-18-0072.1, 2019.